JACS
JOURNAL OF THE AMERICAN CHEMICAL SOCIETY
pubs.acs.org/JACS
Perspective

Advanced Fluorescence Imaging Technology in the Near-Infrared-II Window for Biomedical Applications

Chunyan Li,[‡] Guangcun Chen,[‡] Yejun Zhang, Feng Wu, and Qiangbin Wang*

Cite This: *J. Am. Chem. Soc.* 2020, 142, 14789−14804
Read Online
ACCESS | Metrics & More | Article Recommendations

ABSTRACT: Fluorescence imaging has become a fundamental tool for biomedical applications; nevertheless, its intravital imaging capacity in the conventional wavelength range (400−950 nm) has been restricted by its extremely limited tissue penetration. To tackle this challenge, a novel imaging approach using the fluorescence in the second near-infrared window (NIR-II, 1000−1700 nm) has been developed in the past decade to achieve deep penetration and high-fidelity imaging, and thus significant biomedical applications have begun to emerge. In this Perspective, we first examine recent discoveries and challenges in the development of novel NIR-II fluorophores and compatible imaging apparatuses. Subsequently, the recent advances in bioimaging, biosensing, and therapy using such a cutting-edge imaging technique are highlighted. Finally, based on the achievement in the representative studies, we elucidate the main concerns regarding this imaging technique and give some advice and prospects for the development of NIR-II imaging for future biomedical applications.

INTRODUCTION

Intravital imaging technology provides a favorable approach for achieving insight into the anatomical structures, molecular biomarkers, and physiological activities in living organisms, which opens new avenues of biomedical research and clinical practice.[1] Among various imaging modalities, including computed tomography (CT), magnetic resonance imaging (MRI), ultrasound (US), positron emission tomography (PET), and single-photon-emission CT (SPECT), fluorescence imaging simultaneously features a series of salient merits such as rapid feedback, multiple signal acquisition capability, high sensitivity, and the absence of ionizing radiation; thus, it is one of the fastest developing and most widely used imaging technologies in the biomedical field. However, challenges remain. A major limitation of fluorescence imaging is its restricted tissue penetration depth. Acquiring fluorescence signals is greatly dependent on the interaction between photons and biological tissues, such as reflection, absorbance, scattering, and autofluorescence (Figure 1a).[2] The wavelengths used in classical fluorescence imaging for both excitation and emission are mainly located in the visible range (400−650 nm), where significant absorption and scattering effects induced by biological tissues as well as strong autofluorescence originating from specific biomolecules (e.g., flavins, lipofuscin, reticulin, and exogenous foods) result in low tissue penetration (<3 mm), leading to a significant loss of physiological and pathological information at the whole-body level.

The discovery of the biological-tissue transparency window and advances in near-infrared (NIR) technology suggested exciting prospects for *in vivo* fluorescence imaging. Wavelengths ranging from 650 to 950 nm is the first confirmed biological-tissue transparency window (denoted as the first near-infrared window, or the NIR-I window), and this range exhibits significantly increased tissue penetration compared with visible light, owing to decreased photon absorbance, scattering, and autofluorescence. The NIR-I fluorescence dyes indocyanine green (ICG) and methylene blue (MB) (approved by the U.S. Food and Drug Administration (FDA)) have made significant contributions to clinical diagnostics and interventions,[3,4] especially for fundus angiography and lymphography. Despite this, achieving tissue penetration at the millimeter level in the NIR-I region remains difficult to meet the multilevel and diverse requirements of practical applications. To this end, scientists resurveyed the interactions between photons and biological tissues and executed exploratory research.

In 2009, a pioneering work by Dai at Stanford University revealed a new bioimaging window, commonly termed as the NIR-II window (1000−1700 nm) (Figure 1b),[5,6] which displays superior performance in *in vivo* bioimaging. Compared with the NIR-I region, photon absorption of water in the NIR-II region is somewhat stronger (e.g., 970, 1200, and 1450 nm) due to vibrational overtone bands and combination transitions (Figure 1c). Despite this, decreased tissue scattering and ultralow autofluorescence (nearly zero background when the wavelength is larger than 1500 nm) play predominant roles (Figure 1d,e),[7] enabling unprecedented improvements in detection depth, resolution, and sensitivity. Taking each aspect into consideration, further optimized optical sub-windows NIR-IIa (1300−1400 nm) and NIR-IIb (1500−1700 nm) have been identified.[8] Based on the above-mentioned unique optical properties, there

Received: June 30, 2020
Published: August 7, 2020

https://dx.doi.org/10.1021/jacs.0c07022
J. Am. Chem. Soc. 2020, 142, 14789−14804

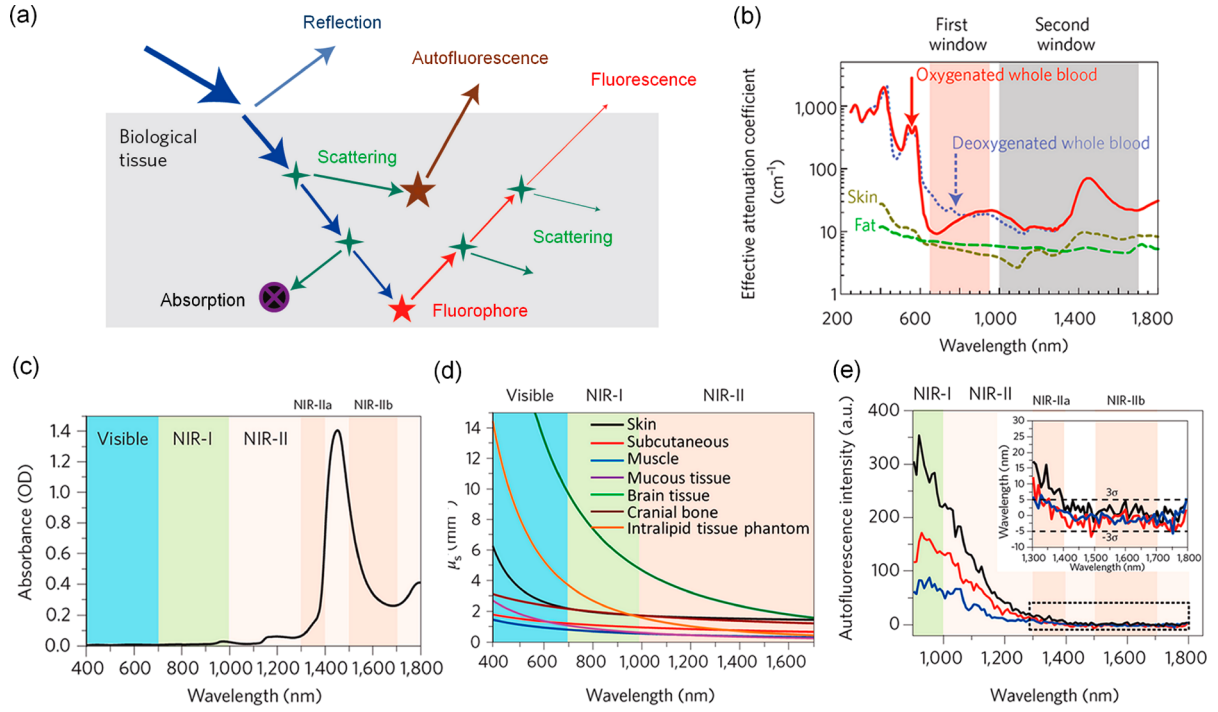

Figure 1. (a) Schematic diagram of the interactions between the photons and tissue when executing fluorescence imaging. (b) Effective attenuation coefficient of various biological components including oxygenated blood, deoxygenated blood, skin, and fatty tissue. (c) Absorption spectrum of water in the range of 400−1800 nm measured through a 1-mm-long path. (d) Reduced scattering of different biological tissues and intralipid solution in the range of 400−1700 nm. (e) Autofluorescence spectra of *ex vivo* mouse liver (black), spleen (red), and heart tissue (blue) under 808 nm excitation. Panels a, c, d, and e reproduced with permission from ref 2. Copyright 2017, Nature Publishing Group. Panel b reproduced with permission from ref 6. Copyright 2009, Nature Publishing Group.

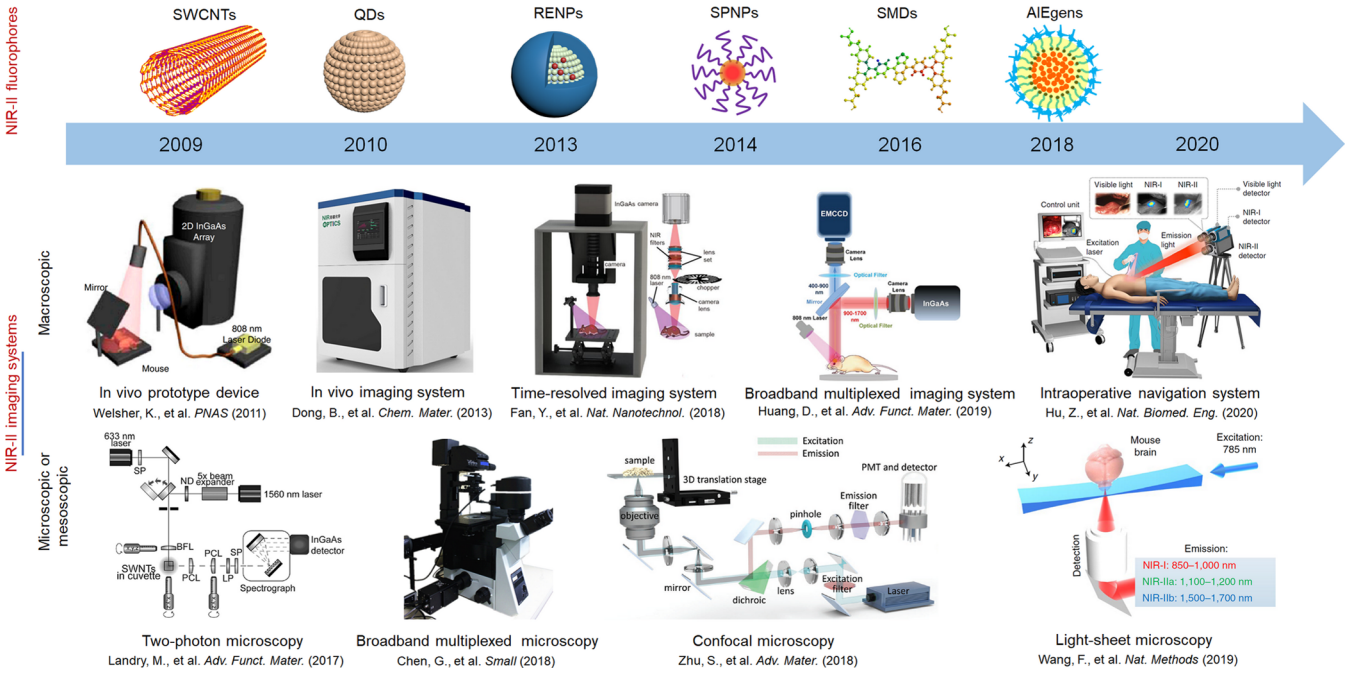

Figure 2. Timeline of major milestones in NIR-II fluorescence imaging technology. Reproduced with permission from ref 22. Copyright 2011, National Academy of Sciences. Reproduced with permission from ref 57. Copyright 2019, Wiley-VCH. Reproduced with permission from ref 58. Copyright 2018, Nature Publishing Group. Reproduced with permission from ref 59. Copyright 2020, Nature Publishing Group. Reproduced with permission from ref 60. Copyright 2017, Wiley-VCH. Reproduced with permission from ref 61. Copyright 2018, Wiley-VCH. Reproduced with permission from ref 62. Copyright 2019, Nature Publishing Group.

has been greatly increased attention focused on the development of novel NIR-II fluorophores, imaging instruments, and biomedical applications in the past decade. In this Perspective, we examine recent discoveries and challenges in the development of novel NIR-II fluorophores and compatible imaging apparatuses, provide representative applications in bioimaging,

https://dx.doi.org/10.1021/jacs.0c07022
J. Am. Chem. Soc. 2020, 142, 14789−14804

biosensing, and theranostic applications, and propose potential solutions and ideas for future research.

NIR-II FLUOROPHORES

The emergence of such a new biological-tissue transparency window has aroused extensive interest in the fields of chemistry, materials science, and biology. The design and construction of NIR-II fluorophores based on organic, inorganic, and hybrid-material systems have achieved a substantial progress in the past decade. Representative fluorescent materials (Figure 2), including single-walled carbon nanotubes (SWCNTs),[5] quantum dots (QDs),[9−12] rare earth-doped nanoparticles (RENPs),[13−15] semiconducting polymer-based nanoparticles (SPNPs),[16,17] small-molecule dyes (SMDs),[18−20] and aggregation-induced emission luminogens (AIEgens),[21] have greatly extended the arsenal of currently available fluorophores for biomedical applications.

SWCNTs. SWCNTs are a type of 1D carbon nanomaterial that is formed from a single sheet of graphite composed of carbon in a honeycomb lattice and rolled into a tube with a diameter ranging from sub-nanoscale to several nanometers. In addition to special physical and chemical properties such as Raman scattering and UV/visible/NIR absorption, SWCNTs also display intrinsic fluorescence in the NIR-II window owing to van Hove transitions across bandgaps. SWCNTs were first employed by Dai et al. as NIR-II nanoprobes by phospholipid-polyethylene glycol functionalization for intravital fluorescence imaging.[5] Subsequently, a series of biomedical studies were conducted with SWCNTs, and some important advances have been achieved.[8,22−27] For example, Belcher and co-workers have demonstrated that the filamentous M13 virus could be used as stabilizer to achieve good dispersion of SWCNTs in aqueous solution.[25] Furthermore, by displaying ovarian cancer targeted peptides SBP, this targeted nanoprobe (SBP-M13-SWCNTs) exhibited higher signal-to-noise ratio compared with visible and NIR-I dyes for *in vivo* detection of tumor nodules. Mukhopadhyay et al. fabricated a specific DNA-wrapped SWCNT and demonstrated its feasibility to determine the therapeutic response of pancreatic ductal adenocarcinoma by precisely monitoring H_2O_2 in the lesion locations.[27] Typically, strong polydisperse infrared absorbance of SWCNTs weakens the NIR-II emission, resulting in low quantum yield (QY) less than 3% as well as accompanying thermal effect. Thus, increasing the QY once sacrificed for avoidance of self-absorption and improving biocompatibility will be the major focuses of future research into SWCNTs.

QDs. QDs are semiconductor nanocrystals (NCs) with diameters in the range of 2−10 nm and display unique optical properties when their radii are smaller than the exciton Bohr radius. Since they were first introduced for biomedical studies by Alivisatos and Nie in 1998,[28,29] QDs have enjoyed great success in *in vitro* analysis and diagnosis. To gain NIR-II emitting QDs, one fundamental principle is to reduce their bandgap, thereby decreasing the energy of an electron jumping from the ground state valence band to an excited state conduction band. By manipulating chemical components, narrow bandgap QDs can be obtained, which are mainly located in groups IV−VI, III−V, II−VI, and I−VI. However, most of these QDs contain highly toxic components such as Hg, Pb, and Cd, resulting in potential toxicity in biomedical applications.

One of the most important advances in fabrication of biocompatible NIR-II QDs was reported by Wang et al. in 2010.[9] They first reported Ag_2S QDs with favorable NIR-II fluorescence by thermal decomposing a single-source precursor of $Ag(DDTC)[(C_2H_5)_2NCS_2Ag]$. Thereafter, a series of high-quality Ag_2S QDs with high QY (approximately 20%) and tunable fluorescence emission ranging from 900 to 1250 nm were obtained.[30,31] Compared with Ag_2S QDs, Ag_2Se QDs have a narrower bandgap (∼0.15 eV) and exhibit great promise for fluorescence emission at longer wavelength. In 2013, the same group developed such a new type of NIR-II QDs by facile solvothermal synthesis; after a coating of C18-PMH-PEG, Ag_2Se QDs displayed good dispersibility in aqueous solution when emission was centered at 1300 nm.[10] Such novel QDs containing no toxic heavy metal components exhibit high chemical stability and hold great potential in biomedical applications. In addition, despite existing concerns over heavy metal ions, some effective strategies have been executed to alleviate these problems and improve the optical properties of QDs at the same time. Most recently, Bawendi and co-workers fabricated InAs-based core/shell (CS) and core/shell/shell (CSS) QDs, which displayed narrow and size-tunable emission in the NIR-II window and a remarkably high emission QY by up to 30% in aqueous solution.[12] Aside from constructing a CS to avoid heavy metal ion leakage, biomacromolecule wrapping also provides an alternative approach. Whey protein and ribonuclease-A were introduced onto the surface of the PbS QDs as shield layers to avoid interaction between QDs with biointerfaces, minimizing their toxic effects.[32,33] Such strategies may be effective for obtaining various biocompatible QDs containing heavy metal. Even so, nontoxic QDs with high QY deserve more attention in the future studies.

RENPs. Generally, RENPs are composed of an inorganic crystalline host matrix and trivalent lanthanide ions (Ln^{3+}) embedded in the host lattice. The process of fluorescence generation in RENPs is due to the resonant transfer of energy from a sensitizer to a rare earth (RE)-activator dopant. By regulating different Ln^{3+} components, it can obtain specific upconversion or downconversion luminescence. In the past two decades, some researchers including Prasad, Liu, Li et al., have focused on the upconversion luminescence property of RENPs and made tremendous efforts for bioimaging.[34−41] To achieve efficient downconversion luminescence in the NIR-II window, aside from the host matrix, the appropriate sensitizers and activators should be taken into account. Because of their large absorption cross sections in the NIR-I region, Nd^{3+}, Yb^{3+}, and Er^{3+} can serve as efficient sensitizers; additionally, Pr^{3+}, Nd^{3+}, Ho^{3+}, Er^{3+}, and Tm^{3+} with ladder-like energy levels are often used as activators in the NIR-II region. Moghe and co-workers fabricated a series of CS structure RENPs, containing rare earth ion-doped $NaYF_4$ as the core and undoped $NaYF_4$ as the shell layer, and achieved tunable multispectral emissions (e.g., 1185, 1310, 1475, and 1525 nm).[13] Zhang et al. developed a β-$NaGdF_4/Na(Gd,Yb)F_4$:Er/$NaYF_4$:Yb/$NaNdF_4$:Yb core/shell1/shell2/shell3 (C/S1/S2/S3) multishell NCs by epitaxial seeded growth. The synthesized probe can efficiently transfer 800 nm near-infrared to 1525 nm short-wavelength infrared via a down conversion process.[14] Prasad et al. demonstrated a hybrid organic−inorganic system consisting of CSS RENPs with organic dye ICG attached on the surface. Thus, the hybrid probe can possess a broadly excitable spectral range (700−860 nm) and a significantly improved NIR-II fluorescence emission with a QY of ∼13%.[15] Despite their great potential for bioimaging, improving the water solubility and avoiding Ln^{3+} concentration quenching effect of RENPs remain to be solved.

https://dx.doi.org/10.1021/jacs.0c07022
J. Am. Chem. Soc. 2020, 142, 14789−14804

Organic Fluorophores. As is well-known, the photoluminescence properties of SMDs are highly correlated with the chemical structures of the molecules created through π interactions. In the past decades, great efforts have been made to tailor the fluorescence emission of small molecules in the NIR region, and a series of NIR-emissive dyes with molecular skeletons such as cyanine, BODIPY, rhodamine, porphyrin, and squaraine have been designed and synthesized. Among them, cyanine- and donor−acceptor−donor (D-A-D)-based structures hold great promise for construction of NIR-II fluorophores.[42−47] Cyanine dyes contain polymethine bridges between two nitrogen atoms with a delocalized charge. Prolonging the conjugated structures or tuning the chemical substitutions are effective approaches to reduce the energy gap between the ground state and the excited state, thereby achieving the red-shift of emission to NIR-II region. In 2016, Dai et al. reported the first D-A-D structure-based small-molecule dye with bright NIR-II fluorescence emission and a QY of 0.3%, CH1055, in which aromatic units conjugated with a D-A-D structure and a benzobisthiadiazole core contribute to NIR-II fluorescence.[18] After that, a series of SMDs have been developed to further improve the QY, water solubility, and biocompatibility of SMDs.[19,20,42−47] For instance, a small-molecule fluorophore FD-1080 with a heptamethine structure was designed by Zhang's group for NIR-II imaging in 2018. After combining with fetal bovine serum, the QY of FD-1080 significantly increased to 5.94%. The high QY of FD-1080 makes it promising for noninvasive high-resolution deep-tissue imaging.[19] Now, a number of NIR-II SMDs are commercially available; however, they are mostly hydrophobic. In 2020, Kilian et al. developed a facile formulation strategy to prepare NIR-II SMDs for injection by simply dissolving them in biocompatible surfactants. By testing 13 hydrophobic NIR-II SMDs, they found the benzo indole butyl diphenylaminocyclopentene heptamethine tetrafluoroborate in Kolliphor HS15 showed the best performance.[20]

In contrast to the aforementioned SMDs, the organic semiconducting materials (SPNPs) have been widely used in electronic components, e.g. organic field-effect transistors (OFETs), organic light-emitting diodes (OLEDs), solar cells (organic photovoltaic, OPV), etc. Their introduction into biomedical imaging has already proven to be successful. Nevertheless, how to tune the spectrum into the NIR-II window is still a challenge. One effective strategy is prolonging the π-conjugation length by designing quinoid stabilized D−A polymers, which can reduce the energy bandgap and result in the spectrum red-shift into the NIR-II window. Pu et al. have explored a series of organic semiconducting-based NIR-II probes with a QY of approximate 2.2%, which have been successfully applied in various intravital biomedical studies, including molecular detection, dynamic monitoring and evaluation of renal function, and imaging-guided precise tumor ablation.[48−51]

Unlike common organic materials with the aggregation-caused quenching (ACQ) property, AIEgens are a class of heterodox molecules that display intense fluorescence emission by aggregate formation, thereby restricting their intramolecular motions. Since the first report by Tang's group in 2001,[52] AIEgens have attracted extensive attention in biomedical field and have been widely used in biolabeling, diagnosis, and imaging. Most recently, novel NIR-II AIEgens have been developed, and such fluorophores exhibit favorable optical advantages such as a high photobleaching threshold, an improved signal-to-noise ratio, the fluorescence turn-on nature, the optimal QY (0.18%−14.8%), etc.,[21,53,54] which further expands the library of NIR-II fluorophores for different studies.

The rapid development of NIR-II fluorophores in the past decade has provided rich probes for biomedical imaging.[2] Each NIR-II fluorophore has its advantages and disadvantages, which should be taken into account for different studies. For photostability, inorganic probes, including SWCNTs, QDs, and RENPs, generally possess better photostability than organic probes. For QY, among the available NIR-II fluorophores, the one with the highest QY is currently the QD-based probe.[55] However, the QY of each NIR-II probe is still much lower than that of its corresponding type of probe emitting in the visible range. And there is plenty of room for further improving their QYs. For biocompatibility, metal element-containing inorganic probes (such as QDs and RENPs) have concerns about the toxicity caused by the release of metal elements, inorganic probes also have concerns about generating a large number of oxidative free radicals and causing toxicity during imaging. For pharmacokinetic, several SMDs can be rapidly eliminated through the renal route, so there is a low residual risk after imaging.[18] And nanoprobes are more likely to be captured by the reticuloendothelial system, thus requiring a long elimination process.[56]

NIR-II FLUORESCENCE IMAGING SYSTEMS

The NIR-II imaging system is another indispensable element for fluorescence bioimaging because it can efficiently collect NIR-II emission signals from NIR-II fluorophores, thereby providing precise anatomical, functional, and molecular images. Unlike the traditional fluorescence imaging apparatuses which could be easily obtained from commercial channels, as an emerging imaging technology, lack of compatible NIR-II imaging systems and components was a major issue. Specifically, previous studies of fluorescence imaging in biomedical areas focused primarily on the visible region, where the photodetectors with a high QY, such as a charge-coupled device (CCD) or a complementary metal oxide semiconductors (CMOS) camera, are available. However, such silicon-based detectors display ultralow quantum efficiency at wavelength >1000 nm, which makes it unsuitable for NIR-II imaging. The emergence of shortwave infrared (SWIR) cameras based on semiconductor alloys with narrower band gaps, such as InGaAs and HgCdTe, make NIR-II imaging possible.

Dai's group built the first intravital NIR-II imaging prototype device,[22] which was mainly composed of a liquid-nitrogen-cooled InGaAs detector (320 × 256 pixel), a diode laser coupled to a collimator with a focal length of 4.5 mm as well as appropriate filter sets and objective lens. This home-built NIR-II imaging device provided high-quality fluorescence images and dynamic videos at the whole-animal level that benefitted from the advantageous photophysical properties of the NIR-II region. Meanwhile, Wang's group began to develop an NIR-II imaging system based on a two-dimensional InGaAs detector (640 × 512 pixel), and continuous efforts were put forth to improve its performance.[10,57] Subsequently, various novel NIR-II imaging systems including broadband (400−1700 nm) multiplexed *in vivo* imaging system, time-resolved *in vivo* imaging system, intraoperative navigation system, confocal microscopy, two-photon microscopy, broadband multiplexed microscopy, and light-sheet microscopy have been developed, providing *in vivo* biological information from macroscopic[22,57−59] to mesoscopic and microscopic scale (Figure 2).[60−63]

https://dx.doi.org/10.1021/jacs.0c07022
J. Am. Chem. Soc. 2020, 142, 14789−14804

Among the latest developed macroscopic NIR-II imaging systems, the design and integration of multiple functional modules have greatly expanded the functions of the NIR-II imaging system. In 2018, Zhang's group reported a time-resolved NIR-II imaging system by coupling a customized time-gating module to a cooled InGaAs camera.[58] This imaging system offered a possibility to perform time-domain multiplexing NIR-II imaging using probes with engineered luminescence lifetimes. In 2019, Wang's group designed a broadband (400−1700 nm) multiplexed imaging system by integrating Si-based CCD for visible and NIR-I imaging and SWIR InGaAs camera for NIR-II imaging.[57] This system can be used to perform fluorescence imaging from visible to NIR-II region and bioluminescence imaging, thus providing great opportunities to simultaneously monitor multiple structural and functional information on organisms by using different imaging channels. More recently, Tian et al. developed a visible and NIR-I/II multispectral imaging instrument for image-guided tumor surgery in patients suffering from liver cancer.[59] The visible and NIR-I/II multispectral imaging can provide accurate tumor boundary information for surgeons to achieve precise tumor surgery. And the development of this equipment opens up a possibility of applying NIR-II imaging in the clinic.

In contrast to the above-mentioned macroscopic imaging systems, confocal and two- or multi-photon (2P/MP) microscopy are powerful tools for the investigation of micro-species. Compared with wide-field imaging setups, confocal microscopy can obtain high-clarity images with a horizontal resolution up to the diffraction limit by focusing its laser beam inside the specimen and using a pinhole to effectively block photons from out-of-focus regions from entering the detector. By scanning the sections at different tissue depths, three-dimensional images are obtained. To acquire high-resolution NIR-II microscopic imaging, a NIR-II confocal microscope was successfully developed by designing and optimizing the NIR excitation source, the IR compatible optical lens, and the NIR photomultiplier diode (PMT) of confocal microscope by Zhu and co-workers in 2018.[61] The 2P/MP microscope is another kind of microscopic imaging instrument using focused femtosecond laser pulses as the excitation source. In the 2P/MP microscope, the beam energy can be concentrated within the spatially confined area of the focus point to generate a substantial signal based on 2P/MP absorption. In 2017, Landry and co-workers developed a dual near-infrared 2P microscope by optimizing excitation and emission wavelengths. In this case, besides a CW 633 nm He−Ne laser, a 1560 nm femtosecond pulsed erbium laser was also used for 2P illumination, which overcame traditional limitations in deep-tissue fluorescence microscopy and demonstrated its great promise for neurotransmitter imaging of a living brain.[60] Taking advantage of reduced photon absorption, scattering, and negligible tissue autofluorescence in the NIR-II window, such novel confocal and 2P microscopy provide powerful tools for investigating the structure, function and molecular events in living bodies.

It should be noted that considering most of the endogenous labeling agents such as fluorescent proteins whose fluorescence spectra locate in the visible and NIR-I regions, Wang's group has developed a broadband microscopy by incorporating Si-based CCD and SWIR InGaAs camera into one system and revealed the location of QDs endocytosed by cells by colocalization imaging of the green fluorescence of the enhanced green fluorescent protein (EGFP) and the NIR-II fluorescence of Ag_2S QDs in cells.[63]

Aside from the macroscopic and microscopic scopes, there is plenty of room for biomedical studies on the mesoscopic scale, especially in brain science. Dai and co-workers developed NIR-II light-sheet microscopy (LSM), achieving long-wavelength excitation and emission up to approximately 785−1320 nm and 1000−1700 nm, respectively.[62] With organic dyes and PbS/CdS core/shell QD probes, they achieved volumetric imaging of glycerol-cleared mouse brain tissue of up to 10 mm^3 with a penetration depth of ∼2 mm. Furthermore, in cases of mouse brain tumors and traumatic brain injury (TBI), NIR-II LSM exhibited favorable capabilities for noninvasive 3D observation of abnormal tumor microcirculation, inflamed immune cell recruitment to the injured region as well as immune checkpoint proteins in living mice.[62]

Although such emerging NIR-II setups represent remarkable methodological advances and have made significant contributions to the biomedical field, even have been used in clinical trials,[59] several technical challenges remain. *First, the absence of SWIR cameras with high resolution and sensitivity.* The quality of SWIR focal plane array (FPA) chips is limited by the available technology. For coupling the light-receiving photodiodes (InGaAs or HgCdTe layer) and the readout circuit (Si layer), traditional approaches use bump connections that are necessary to secure a certain bump pitch, resulting in difficulty to obtain smaller pixel size. SWIR detectors with mainstream availability are 640 × 512 pixels, which cannot compare with the current CCD or CMOS sensors with pixels of million to tens of million. Another major challenge of the SWIR detector is the relatively poor quantum efficiency (QE), which could not achieve high-sensitive imaging in a broad range of wavelengths from 900 to 1700 nm. Therefore, future efforts should be devoted to improving the QE and achieving pixel miniaturization of SWIR chips. *Second, the limitations of the illumination mode.* As a preferred illumination approach, NIR lasers currently serve as the excitation source for NIR-II imaging due to their high power and monochromaticity. Despite this, a major challenge of the NIR laser's illumination is conversion of the Gaussian beam to a flattened beam to achieve even illumination for large samples like whole animals. With the development of beam shaping techniques, this issue is expected to be resolved in the near future. Furthermore, utilization of multilight source or ring-light source strategies may further improve the illumination effect. *Third, the absence of software algorithms.* SWIR imaging was first applied in military and industrial areas. After introduction into the biomedical field, signal processing and image acquisition need to be redesigned to eliminate the undesirable thermal noise often associated with NIR-II imaging and improve the signal-to-noise ratio. Thus, an appropriate software algorithm needs to be formulated. In addition, the development of high cutoff filters and high numerical aperture NIR focusing lenses associated with different imaging implementations is also to be considered.

RECENT ADVANCES OF NIR-II FLUORESCENCE IMAGING IN BIOMEDICAL APPLICATIONS

With the development of novel NIR-II fluorophores and imaging instruments, NIR-II imaging has emerged as a powerful tool in biomedical research. Herein, we give some representative studies of NIR-II imaging-based biomedical research, including bioimaging, biosensing, and theranostic applications.

NIR-II Bioimaging. *Structural Imaging.* Due to its deep tissue penetration depth and high spatial resolution, NIR-II imaging is a promising method for *in vivo* imaging of the fine structure of living tissues, such as the blood vascular system,

https://dx.doi.org/10.1021/jacs.0c07022
J. Am. Chem. Soc. 2020, 142, 14789−14804

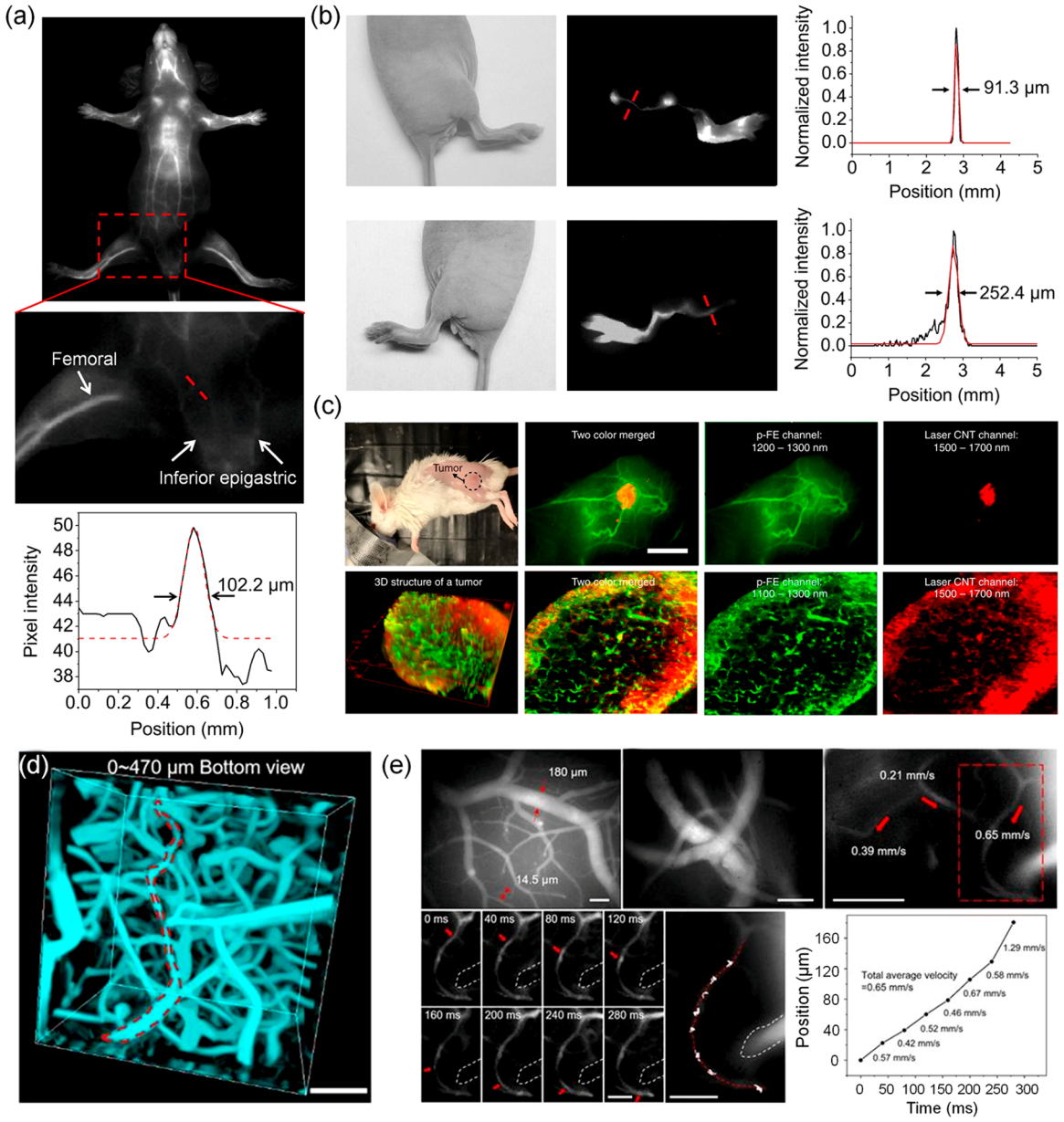

Figure 3. Structural and functional imaging using NIR-II emitting fluorophores. (a) Whole-body blood pool imaging of the nude mouse using NIR-II emitting Ag_2S QDs. (b) Comparative study of Ag_2S QDs (1200 nm, NIR-II) (upper) and ICG (835 nm, NIR-I) (below) for *in vivo* lymphatic imaging. (c) Two-color fluorescence imaging of tumor vasculatures and tumor tissues in the NIR-II window. p-EF channel: tumor vasculatures; CNT channel: tumor. (d) A 3D confocal image of cerebral blood vessels of the rhesus macaque. Bars: 100 μm. (e) *In vivo* imaging of blood flow velocities of the rhesus macaque using a wide-field NIR-II microscopy. Panels a and b reproduced with permission from ref 65. Copyright 2014, Elsevier Inc. Panel c reproduced with permission from ref 72. Copyright 2018, Nature Publishing Group. Panels d and e reproduced with permission from ref 68. Copyright 2020, Theranostics.

lymphatic system, and tumors.[61,62,64−69] Recently, NIR-II probes with high photochemical stability and a long blood circulation time showed numerous advantages in vascular imaging. In 2012, a mouse hindlimb vascular structure was successfully imaged down to ~30 μm using SWCNTs as the fluorophores.[23] In Wang's group, polyethylene glycol (PEG)-capped Ag_2S QDs with a long circulation time (circulation half-time = 4.1 h) were synthesized for blood vascular imaging. In their study, peripheral vasculature (~100 μm) and brain microvasculature (~24.3 μm) were clearly imaged *in vivo* with a micrometer resolution (Figure 3a).[65,70] In addition, the bright NIR-II AIEgens developed by Tang's group also showed as an excellent probe for imaging the blood vessels in hindlimb and scalp.[53,71] With the development of wild-field and confocal NIR-II microscopy, a much better spatial resolution has been achieved during blood vascular imaging. In Dai's group, 3D imaging of vasculatures with a depth of ~1.3 mm and a spatial resolution of sub-10 μm in the brains of mice were obtained using an organic fluorophore named p-FE.[72] In addition to small rodents, *in vivo* cortical vasculature imaging has also been achieved in nonhuman primates by Qian's group.[68] In their study, a microvessel with a diameter of 6.6 μm and the 3D structure of cerebral blood vessels of rhesus macaque were clearly imaged using NIR-II fluorescence confocal microscopy (Figure 3d).

https://dx.doi.org/10.1021/jacs.0c07022
J. Am. Chem. Soc. 2020, 142, 14789−14804

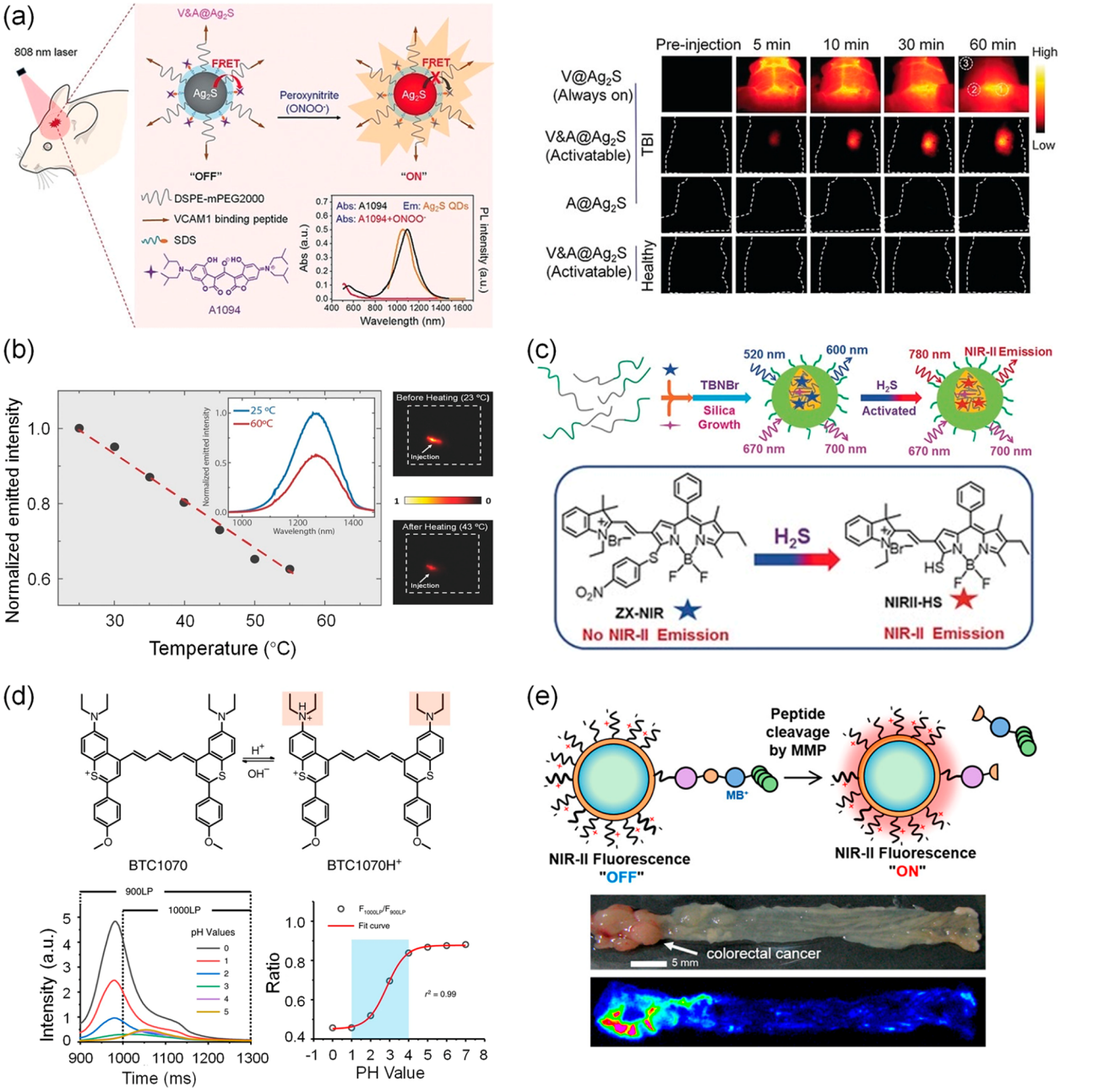

Figure 4. Activatable NIR-II probes for biological sensing. (a) The $ONOO^-$-activatable V&A@Ag_2S probe for *in vivo* detection of traumatic brain injury. (b) Temperature sensing by a core/shell/shell PbS/CdS/ZnS QD emitting in the NIR-II window (1270 nm). (c) pH sensing by pentamethine cyanine fluorophores (BTCs). (d) A H_2S-activated ratiometric fluorescence nanoprobes containing a H_2S-activable boron-dipyrromethene (ZX-NIR) dye and an aza-BODIPY (aza-BOD) dye. (e) The MMP-activatable PbS/CdS/ZnS core/shell/shell QDs for colorectal tumor detection. Panel a reproduced with permission from ref 88. Copyright 2020, Wiley-VCH. Panel b reproduced with permission from ref 90. Copyright 2015, Wiley-VCH. Panel c reproduced with permission from ref 91. Copyright 2018, Wiley-VCH. Panel d reproduced with permission from ref 93. Copyright 2019, Nature Publishing Group. Panel e reproduced with permission from ref 94. Copyright 2017, American Chemical Society.

In addition to the blood vessel system, the lymphatic system imaging is also widely used in clinical trials.[73] Currently, NIR-II imaging offers the possibility of *in vivo* imaging lymphatic system in deep tissues with high clarity.[44,65] For example, research by Wang's group showed the Ag_2S QD was a stable NIR-II fluorophore for imaging the lymphatic system with a better resolution and deeper penetration depth than ICG-based NIR-I imaging (Figure 3b).[65] Similarly, Antaris et al. comparatively analyzed lymph node imaging in deep tissue (~5−8 mm depth) with NIR-II emitting organic dye (CH-4T) and NIR-I emitting ICG.[44] Their results illustrated the unique advantages of NIR-II imaging for *in vivo* detection of deep anatomical features of the lymphatic system.

Structural imaging of tumors is also gaining the interest of researchers for its crucial role in exploring the mechanisms of tumorigenesis as well as the diagnosis and treatment of tumors. Currently, NIR-II imaging has been extensively used in early diagnosis of tumors with a high tumor-to-background ratio (TBR).[30,74−76] More recently, the development of multichannel NIR-II imaging and the 3D light-sheet imaging techniques has greatly promoted assays of tumor structure. In 2018, Wan et al. obtained the 3D structure of 4T1 tumors in

https://dx.doi.org/10.1021/jacs.0c07022
J. Am. Chem. Soc. 2020, 142, 14789−14804

living mice by two-channel NIR-II confocal microscopy.[72] In this study, the vasculatures of tumors were highlighted by p-FE emitting 1100−1300 nm, and the tumors were highlighted by CNTs emitting 1500−1700 nm (Figure 3c). Thus, the internal structures of the tumor were clearly identified; this showed an abundance of blood vessels exist around and in the tumor to fuel tumor growth.

Functional Imaging. In addition to portraying the fine structures of deep tissues, NIR-II imaging is also a powerful tool to analyze the functions of cells and tissues.[16,68,77,78] Currently, real-time monitoring of blood flow and heart rate are the most important applications of NIR-II functional imaging.[16,68,78] In 2014, Hong et al. developed a NIR-II method for real-time monitoring of mouse arterial blood flow via a pDA dot (E_m = 1047 nm).[16] With high speed NIR-II imaging (>25 frames per second), the highest instantaneous blood velocity and the lowest instantaneous blood velocity were accurately measured to be ∼8 cm s^{-1} and ∼2 cm s^{-1}, respectively. In addition, the heart rate was also successfully measured to be 290 beats per minute in mice. In 2019, Dai's group observed the on−off, intermittent, and reversed blood flow in the tumor using a light-sheet imaging system.[62] In 2020, Qian's group successfully monitored the blood flow velocity of capillaries and the cardiac impulse period in macaque monkeys by using a high speed wide-field microscope (25 frames per second).[68] Then, a blood flow velocity of approximately 0.65 mm/s was accurately calculated by NIR-II imaging (Figure 3e). In view of the excellent temporal resolution, NIR-II imaging has possible applications in the diagnosis and evaluation of various cardiovascular diseases.

These novel 2D, 3D, and multi-channel NIR-II imaging techniques offer the opportunity to perform *in vivo* assays of the fine structures and functions of deep tissues at macroscopic, mesoscopic, and microscopic levels. The development of clinically available NIR-II probes with high safety and high QY is currently the main challenge of NIR-II fluorescence-based bioimaging. It is believed that, with further development of clinically available NIR-II fluorophores, NIR-II imaging will be a promising alternative to traditional optical imaging for *in situ* and high-fidelity structural and functional imaging in the clinic.

NIR-II Biosensing. In the past several years, another significant advance in NIR-II imaging research was the development of activatable NIR-II fluorophores for biosensing.[77,79−81] Activatable NIR-II fluorophores can alter their fluorescence intensity or emission wavelength according to specific microenvironment parameters, thus showing higher signal-to-background ratio, higher sensitivity, and better specificity than "always-on" fluorophores. So far, NIR-II fluorophores that can sense reactive oxygen species (ROS), reactive nitrogen species (RNS), reactive sulfur species (RSS), temperature, gas, pH, or a specific enzyme have been developed, offering possibilities for deciphering the biological activities of cells and tissues at the molecular level.[80,81]

ROS/RNS/RSS Sensing. The imbalance of the redox environment in the organism is related to the occurrence and development of many diseases, such as cancer, tissue injury, infection, etc.[81−83] Currently, several NIR-II fluorophores have been developed to monitor the redox status in organisms, including ROS, RNS, and RSS.[81,84,85]

In 2018, Chen and co-workers synthesized H_2O_2-responsive $NaCeF_4$:Er/Yb NCs for uric acid detection.[84] In this system, H_2O_2 reacted with Ce^{3+} ions in $NaCeF_4$:Er/Yb NCs, thus quenching NIR-II emission of $NaCeF_4$:Er/Yb NCs. For RNS, several organic and inorganic $ONOO^-$-responsive NIR-II probes have been developed. In Zhang's group, a peroxynitrite activatable organic probe (named IRBTP-B) was designed for drug-induced hepatotoxicity monitoring.[86] Furthermore, the same group developed a panel of fluorescent dyes (CX) to sense $ONOO^-$ via the principle of Förster resonance energy transfer (FRET) between CX dyes.[87] In addition to the organic dyes, a QD-based $ONOO^-$-activatable probe was recently developed via a FRET principle in Wang's group for TBI imaging.[88] In this system, the $ONOO^-$-responsive A1094 chromophore was conjugated with Ag_2S QDs to generate the V&A@Ag_2S probe (Figure 4a). Due to the FRET between Ag_2S QDs and A1094, the intact V&A@Ag_2S remained quenched. After exposure to $ONOO^-$, A1094 was rapidly bleached, and the NIR-II fluorescence of Ag_2S QDs was turned on. For RSS, Fan's group developed hyaluronidase and thiols cooperatively activatable NIR-II fluorescence nanoprobes (HISSNPs) for ultrahigh specific tumor imaging.[89] In their study, HISSNPs were synthesized by locking the fluorescence-quenched IR-1061 aggregation in hyaluronic acid chains and disulfide bonds. Thus, the fluorescence of HISSNPs could be turned on via unlocking the hyaluronic acid chains and disulfide bonds by hyaluronidase and GSH, respectively.

Temperature Sensing. Temperature is one of the most important physiological parameters of organisms. In 2015, Vetrone and co-workers synthesized a core/shell/shell PbS/CdS/ZnS QD emitting in the NIR-II window (1270 nm).[90] In this study, strong temperature-dependent emission intensity variation of PbS/CdS/ZnS QDs was observed (Figure 4b). With temperatures varying between 20 and 70 °C, a sensitivity of 1% per °C was found, suggesting the promise of QDs for sensing the temperature in biological systems. Then, an *ex vivo* study in chicken breast tissue suggested the temperature of tissues can be measured by thermal-sensitive QDs at a tissue depth of 1 cm. This study opens the possibility of sensing biological temperature in deep tissues by NIR-II imaging.

Gas Sensing. Biological gases, such as hydrogen sulfide (H_2S) and NO, are also associated with many pathological processes. In 2018, Xu and co-workers developed H_2S-activated ratiometric fluorescence nanoprobes with NIR-II emission at 900−1300 nm.[91] In their study, a hydrogen sulfide (H_2S)−activable boron−dipyrromethene (ZX-NIR) dye and an aza-BODIPY (aza-BOD) dye were encapsulated in the hydrophobic interior of the core−shell silica nanocomposites (Figure 4c). The ZX-NIR can be activated by H_2S to generate NIR-II fluorescence, and the aza-BOD dye can serve as the internal reference. With the H_2S-activated ratiometric probe, colorectal tumors in animal models can be accurately identified *in vivo*. For NO detection, Strano and co-workers synthesized an alginate-encapsulated SWCNT for *in vivo* sensing of inflammation.[92] In this system, an NO-responsive DNA oligonucleotide ds$(AAAT)_7$ was wrapped in SWCNT to sense NO. Consequently, the fluorescence emission of SWNTs can be gradually quenched by NO, thus detecting the NO level in implantable inflammation.

pH Sensing. pH is a crucial physiological parameter of organisms, and abnormal pH can also be used as a pathological microenvironment feature for the diagnosis and treatment of diseases. Recently, researchers have also developed NIR-II probes for *in vivo* pH sensing. In 2019, Zhang's group reported a series of NIR-II pentamethine cyanine fluorophores (BTCs) that exhibit pH-responsive fluorescence.[93] When pH changed from 5 to 0, a large peak shift from 1065 to 980 nm was observed, suggesting a good ratiometric fluorescence response to pH in BTCs (Figure 4d). Consequently, they successfully applied

https://dx.doi.org/10.1021/jacs.0c07022
J. Am. Chem. Soc. 2020, 142, 14789−14804

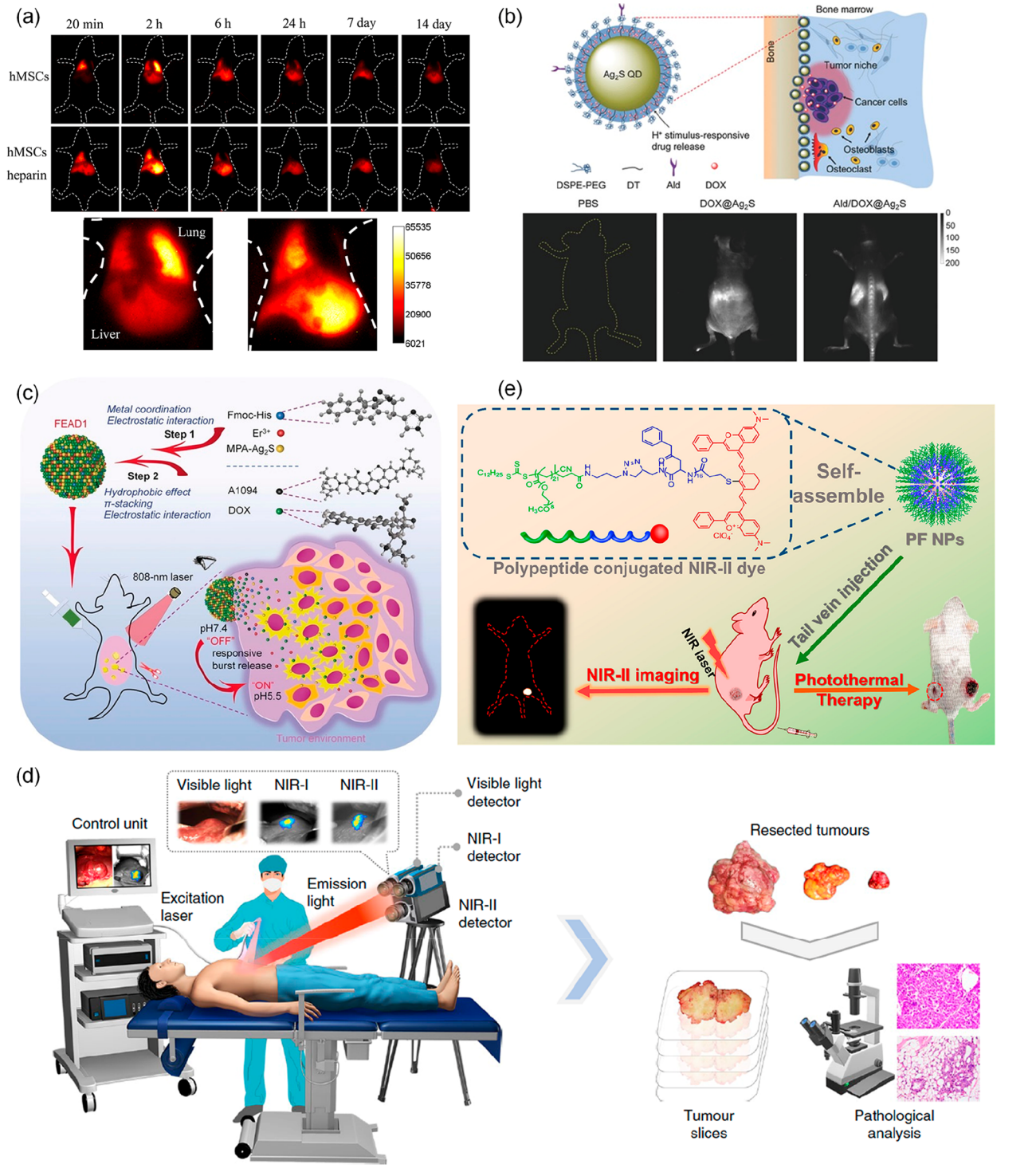

Figure 5. NIR-II imaging-guided therapy. (a) *In vivo* tracking of Ag_2S QD-labeled stem cells for liver regeneration in a mouse with acute liver failure. (b) NIR-II imaging-guided bone-targeted delivery of Ald/DOX@Ag_2S nanodrugs for bone tumor therapy. (c) A tumor microenvironment-activated NIR-II nanotheranostic system (FEAD1) for precise drug release monitoring, diagnosis, and treatment of peritoneal metastases. (d) In-human liver-tumor surgery guided by multispectral optical imaging in the visible and NIR-I/II windows. (e) NIR-II imaging-guided PTT for mammary carcinoma tumor treatment using a macromolecular fluorophore (PF) agent. Panel a reproduced with permission from ref 99. Copyright 2014, Wiley-VCH. Panel b reproduced with permission from ref 105. Copyright 2017, Wiley-VCH. Panel c reproduced with permission from ref 106. Copyright 2020, Wiley-VCH. Panel d reproduced with permission from ref 59. Copyright 2020, Nature Publishing Group. Panel e reproduced with permission from ref 114. Copyright 2019, Wiley-VCH.

BTC1070 for *in vivo* measurement of gastric pH, showing a good measurement accuracy at a depth of up to 4 mm.

Enzyme Sensing. Enzymes, including matrix metalloproteinase (MMP), nitroreductase (NTR), alkaline phosphatase (ALP), caspases, etc., have been widely used to activate fluorescent probes and report pathological processes.[94−96] Currently, several enzyme-activable NIR-II probes have been developed. As a hallmark of the cancer microenvironment,

https://dx.doi.org/10.1021/jacs.0c07022
J. Am. Chem. Soc. 2020, 142, 14789−14804

MMPs are often used as a biomarker for tumor diagnosis and treatment. In 2017, Kim and co-workers developed MMP-activatable PbS/CdS/ZnS CSS QDs for tumor detection (Figure 4e).[94] In this system, the fluorescence of QDs were quenched via a photoexcited electron transfer (PET) quenching process between methylene blue and QDs. In tumor microenvironment, highly active MMP cleaved the linker peptide and released MB, thus turning on the fluorescence of QDs. In another example, Cai and co-workers reported an NTR-triggered NIR-II probe (IR1048-MZ) for solid tumor diagnosis and therapy.[96] In this study, a NIR-II emitting IR-1048 dye was conjugated with a nitroimidazole group (2-(2-nitroimidazolyl)-ethylamine, MZ) to generate IR1048-MZ. Thus, the fluorescence of IR-1048 was quenched via the MZ group induced electron transfer. In the hypoxia microenvironment of a solid tumor, the highly active NTR reduced the MZ group in IR1048-MZ, thus recovering the NIR-II fluorescence of IR1048-MZ.

With the numerous advantages of high SBR, high sensitivity, and excellent specificity, we believe that activatable NIR-II probes will greatly promote the application of fluorescence imaging technologies in the early detection of diseases. To achieve this goal, the NIR-II biosensing technology may need to be further advanced in the following aspects. First, the single physiological parameter-activatable probe will still face non-specific signal interference due to a physiological parameter often appears under different pathological conditions. Thus, the development of NIR-II probes that can be activated by multiphysiological parameters in target tissues may be an effective strategy to further improve the specificity of biosensing. Second, the courses of the disease are often accompanied by dynamic changes of various interrelated physiological conditions. Thereby, the development of multi-channel activatable NIR-II imaging to simultaneously sensing different physiological parameters in a target tissues may be useful for fully disclosing the underlying mechanism of disease occurrence and development.

NIR-II Imaging-Guided Therapeutic Applications. In the past decades, NIR-II imaging technique has greatly promoted the application of fluorescence imaging technology in structural and functional imaging of biological tissues and early detection of diseases. At the same time, due to the low absorption and scattering characteristics of NIR-II light in living tissue, it also provides a new tool for the precise treatment of diseases. Currently, a series of NIR-II-based treatment strategies, including imaging-guided cell therapy, imaging-guided surgery, imaging-guided drug delivery/release monitoring, and imaging-guided PDT/PTT, have been developed and show numerous advantages for precise disease treatment.[74,97,98]

Imaging-Guided Cell Therapy. Cell therapy, including stem cell therapy and immune cell therapy, is bringing a revolution to modern medicine because it shows great potential for the treatment of a series of incurable human diseases, such as cancer, neurodegenerative diseases, and cardiovascular diseases. In the past few years, NIR-II imaging has served as a powerful tool for *in vivo* tracking the fate of cells, exploring the underlying mechanisms of cell therapy, and guiding precision cell therapy.[77,97]

For stem cell tracking, the first whole-body tracking of transplanted stem cells in the NIR-II window was achieved by Wang et al. using the Tat peptide-capped Ag_2S (Tat-Ag_2S) QDs.[99] In their study, Tat-Ag_2S can be used to track 1000 subcutaneously transplanted cells for a period of 30 days. Moreover, due to the high spatiotemporal resolution of NIR-II imaging, the dynamic translocation of transplanted stem cells from the lung to the liver was clearly observed with a temporal resolution of 100 ms (Figure 5a). Thus, in the mouse models of acute liver injury and skin injury, Ag_2S QD-based NIR-II imaging was successfully used to develop cell transplantation strategies to promote the migration of stem cells to the injury site.[99,100] In another example, Yang and co-workers developed a PbS QD-based stem cell tracking strategy for optimizing MSC therapy in a mouse model of the supraspinatus tendon.[101] More recently, multiplexed NIR-II fluorescence/bioluminescent imaging (BLI) methods were developed by Wang's group. Thus, the dynamic translocation, viability, and differentiation of transplanted stem cells can be simultaneously monitored *in vivo*.[57,63]

In addition to stem cell tracking, NIR-II imaging is also promising for immune cell tracking and imaging-guided immunotherapy. In 2018, Hao and co-workers developed a programmable chemotherapy and immunotherapy strategy under the guidance of multiplexed NIR-II imaging. In their study, Ag_2Se QDs (λ_{Em} = 1350 nm) were used to monitor doxorubicin (DOX) and stromal-cell-derived factor-1α (SDF-1α) in the tumor site. After the arrival of DOX and SDF-1α, the fluorescence of Ag_2S QDs (λ_{Em} = 1050 nm) was used to track the chemotactic migration behavior of intravenously transplanted natural killer (NK)-92 in the tumor site. Multiplexed NIR-II imaging offers spatiotemporal distribution information on DOX, SDF-1α, and NK cells in the tumor site, thus facilitating optimization of administered treatments and enhanced tumor therapy.[64]

Imaging-Guided Drug Delivery/Release Monitoring. The targeted delivery and precise release of drugs are major challenges in the field of precise medicine. NIR-II imaging offers a promising tool for *in vivo* monitoring of drug delivery and release, thus facilitating drug development and optimization of drug delivery.[102−106]

In 2017, Li and co-workers reported a Ag_2S QD-based nanodrug (Ald/DOX@Ag_2S) for drug delivery monitoring and bone tumor therapy (Figure 5b).[105] The benefits of dynamic translocation, the deep tissue penetration of NIR-II imaging, and the bone targeting of Ald/DOX@Ag_2S can be monitored in real time, thus helping to design efficient bone tumor therapies with simultaneous stereotactic chemotherapy and inhibition of osteolysis. In addition to guided drug delivery, NIR-II fluorescence can also be used to monitor drug release in target tissues. In 2020, Lin and co-workers reported a tumor microenvironment-activated NIR-II nanotheranostic system (FEAD1) (Figure 5c).[106] In their study, Ag_2S QDs, DOX, NIR absorber A1094, and the peptide Fmoc-His were self-assembled into nanoparticles. Because of the FRET between the Ag_2S QDs and A1094, the NIR-II fluorescence of Ag_2S QDs was quenched in the intact FEAD1. Upon delivery of FEAD1 to the tumor, FEAD1 was disassembled in the acidic tumor microenvironment to release A1094, DOX, and Ag_2S QDs, and thereafter the NIR-II fluorescence of Ag_2S QDs was turned on. In this way, the NIR-II fluorescence of Ag_2S QDs precisely reflects the release of DOX within the tumor tissue, thus facilitating precise tumor theranostics.

Imaging-Guided Surgery. Currently, surgery is the most common strategy for solid tumor treatment. Because of its noninvasive and high spatiotemporal resolution, intraoperative optical imaging has been extensively used to help surgeons perform surgery quickly and precisely. Recently, NIR-II imaging-guided surgery methods have greatly advanced the

https://dx.doi.org/10.1021/jacs.0c07022
J. Am. Chem. Soc. 2020, 142, 14789−14804

accuracy, sensitivity, and specificity of tumor surgery in both animal research and clinical practice.[98,107−109]

For example, Wen and co-workers developed a NIR-II emitting nanochain probe (APP-Ag_2S-RGD) for intraoperative NIR image-guided surgery.[110] Due to geometrically enhanced multivalent targeting, APP-Ag_2S-RGD is more readily taken up by tumor cells than RGD-functionalized Ag_2S QDs, providing a high TBR of 13.6. As a result, tiny metastatic tumor foci (~0.2 mm in diameter) were detected and eliminated under NIR-II imaging guidance. In addition to inorganic nanoprobes, excretable SMDs have also been developed for imaging-guided surgery. In 2016, Antaris and co-workers synthesized a NIR-II emitting organic molecule (CH1055) with a rapid excretion property.[18] In this study, approximately 90% of CH1055 can be excreted through the kidneys within 24 h after injection, thus greatly reducing the potential side effects caused by probe residue after surgery. More recently, the first NIR-II imaging-guided tumor surgery in a human was achieved by Hu and co-workers (Figure 5d).[59] In their study, FDA-approved ICG was used as the fluorophore. Thus, the NIR-I and NIR-II emissions of ICG can be simultaneously detected by different detectors that integrated in an optical-imaging instrument. In a test of liver-tumor surgery in 23 patients, intraoperative NIR-II imaging showed a better tumor detection sensitivity, higher TBR, and higher tumor detection rate than intraoperative NIR-I imaging. With such unique merits, the novel NIR-II imaging strategies may have great potential for improving preoperative diagnosis and intraoperative navigation in the future.

Imaging-Guided PDT/PTT. Light-based therapy, including photothermal therapy (PTT) and photodynamic therapy (PDT), is emerging as a noninvasive, remote-controllable, and highly specific strategy for cancer treatment.[111−116] *In vivo* imaging techniques that can clearly indicate the location and boundaries of the tumor are of great significance for guiding accurate phototherapy.

In 2019, Li and co-workers developed an amphiphilic polypeptide-conjugated NIR-II fluorophore (Flav7) for simultaneous tumor imaging and PTT (Figure 5e).[114] The synthesized macromolecular fluorophore (PF) nanoparticles possessed both NIR-II emission at 1081 nm and high photothermal conversion efficiency (42.3%). By integrating tumor imaging and precise PTT, the diagnostic accuracy and treatment outcomes for a murine mammary carcinoma tumor were distinctly improved. In another example, Gao and co-workers synthesized a lipophilic NIR-II fluorophore (BPBBT) with both twisted intramolecular charge transfer and AIE characteristics. By using the BPBBT-based NIR-II imaging and PTT, the primary orthotopic colon tumor and metastatic lesions in mouse were preciously delineated and treated.[115] In addition to PTT, NIR-II imaging-guided PDT has also been developed. In 2019, Wang and co-workers reported a red blood cell-based multimodal theranostic probe (RBCp) for image-guided tumor surgery and photodynamic therapy.[117] The RBCp can accumulate and stably remain in tumors for approximately 4 h after an intravenous injection, thus offering sufficient time for guiding tumor surgery. In addition, the intratumoral RBCp can be irradiated by an NIR laser to release O_2, thus enhancing the PDT efficiency for metastatic tumors.

Overall, the emergence of NIR-II-guided therapy shows great promise for improving the specificity, efficiency, and safety of disease treatment. It is believed that NIR-II imaging will play an increasingly important role in both accurate diagnosis and precise treatment of diseases. In the future, the development of clinically available NIR-II probes and NIR-II imaging equipment will be needed to promote the therapeutic and theranostic applications of NIR-II imaging in the clinic.

CONCLUSIONS AND PERSPECTIVES

In the 10 years since the concept of NIR-II fluorescence imaging was first proposed, various NIR-II fluorophores and compatible imaging instruments for macroscopic, mesoscopic, and microscopic scales have been developed, providing powerful tools for biomedical applications. However, such a cutting-edge imaging technology is still at a relatively early stage in its development, and some essential issues should be resolved before its substantial and extensive applications in preclinical studies and clinical practice. In the following points, we elucidate the main concerns regarding this imaging technique and give some advice and prospects for the development of NIR-II imaging for future biomedical applications.

NIR-II Fluorophores. In view of their bioapplications, the first and foremost issue is the biosafety of NIR-II fluorophores. Some important qualities should be met such as outstanding optical properties, facile functionalization, and good compatibility. At the same time, developing novel strategies for endogenous labeling should also be taken into account.

(1) Decent biocompatibility. Aside from applications in preclinical studies and *in vitro* assays, they are crucial to achieving NIR-II clinical translation. The arsenal of NIR-II fluorescence probes has expanded substantially in the past decade. Despite this, to date, there are no FDA-approved NIR-II fluorophores available for clinical use. Thus, when optimizing present probes or designing new NIR-II fluorophores, great effort should be made to make sure that the probes contain nontoxic components. In addition, optimizing the size (<5 nm) and surface coating of probes for rapid renal excretion is another promising way for designing safe probes.

(2) Outstanding optical properties. High fluorescence QY of NIR-II fluorophores is especially important for increasing the sensitivity and broadening the applications of this technology. Most currently available NIR-II fluorophores have a quite low QY, which should be further improved by optimizing the probe in several aspects, such as molar absorption coefficient, electronic transition, surface chemistry, etc. Meanwhile, improvement of chemical and irradiation stability against photobleaching and blinking is another key point to be resolved to ensure the accuracy of imaging data. Simultaneous multiplexed imaging with different fluorophores is often required to investigate complex physiological and pathological processes. To avoid crosstalk, a primary principle for spectrum tuning is to develop NIR-II fluorophores with a large Stokes shift and a sharp emission spectrum with a narrow full width at half-maximum.

(3) Facile functionalization and good compatibility. Besides NIR-II fluorescence architectures, appropriate strategies to introduce functional components to improve the water solubility and targeting capabilities of probes are very important for biomedical applications. In addition, developing multimodal probes by doping or conjugating other contrast agents (such as MRI and CT contrast agents) with NIR-II probes is vital to make NIR-II probes compatible for multimodal imaging or treatment. Therefore, the fact NIR-II fluorophores could be easily modified

https://dx.doi.org/10.1021/jacs.0c07022
J. Am. Chem. Soc. 2020, 142, 14789−14804

while maintaining favorable fluorescence properties is important.

(4) Endogenous labeling. Although abundant NIR-II fluorophores have been developed by various chemical synthesis methods; such exogenous probes are not heritable in living organisms and are not suitable for tracking of long-term and dynamic bioinformation such as gene expression, or cell proliferation and differentiation. Thus, another effort should be focused on development of genetically encoded NIR-II fluorescent proteins to allow better tissue penetration depth, spatial resolution, and sensitivity over currently available fluorescent proteins.

Imaging Systems. Because of the complexity and the dynamic change characteristics of physiological and pathological processes, we should assess them on different spatial and time scales. Despite substantial progress in the area of imaging apparatuses, there are still many important problems to be further solved.

(1) NIR-II real-time multi-channel imaging system. Because of the complexity and dynamic change properties of living organisms, static single-source signal acquisition cannot give the whole profiles of physiological and pathological changes. In this respect, traditional fluorescence imaging has been restricted by temporal resolution and tissue penetration depth. Real-time multi-channel NIR-II imaging systems can simultaneously record multiple events, which might provide wonderful insights into the mysteries of living bodies and the mechanisms of diseases.

(2) NIR-II intravital endoscopy imaging system. As the clinical gold standard of detection, endoscopy dominates examination of interior body cavities, and hollow tissues and organs. Due to the ultralow background signal in the NIR-II region which is nearly zero when the wavelength is greater than 1500 nm, NIR-II endoscopy can achieve ultrahigh sensitivity detection that cannot be achieved using traditional endoscopy. A prototype of NIR-II endoscopy was first reported by Cheng and co-workers; combination with ICG-conjugated bevacizumab (Bev-ICG) showed NIR-II fluorescence and white-light imaging of VEGF at the same time in an orthotopic rat colorectal cancer model.[118] Future iterations should preferentially aim for a "see-and-treat" strategy, that is, diagnosis and treatment synchronization.

(3) NIR-II fluorescence integrated multimodal tomography imaging system. Although there has been substantial progress in the development of NIR-II fluorescence systems in the past decade, a major limitation of *in vivo* imaging is the difficulty of acquiring comprehensive data. Combining modalities has certainly been an area of great interest recently because it could prevent misdiagnosis or loss of valuable information. Another challenge of fluorescence imaging in whole animals is how to achieve precision quantitative analysis. NIR-II fluorescence photons with deep-tissue penetrating capabilities may significantly facilitate 3D tomography imaging. Combined with other imaging technologies, such as MRI and CT, NIR-II imaging could provide powerful tools to parse complex anatomical structures and gain functional information on living bodies.

Future Applications. With the development of novel NIR-II probes and NIR-II imaging systems, NIR-II imaging has become a powerful imaging tool for *in vivo* assays of the structure and function of deep tissues as well as guiding precise therapy. In the future, we believe that NIR-II imaging will aid in a broad range of fundamental and clinical research.

(1) For oncology research, NIR-II imaging offers the possibility for intravital imaging of 3D structures, vasculature distribution, blood flow, and the dynamic immune cell infiltration process in tumors. However, exogenous NIR-II probe-based imaging only provides instantaneous information, and continuous tracking of the entire tumor development process has not been achieved. Further development of multiple spectral imaging methodologies by combining multiple endogenous and exogenous NIR-II probes will offer an exceptional tool for comprehensively analyzing the occurrence, development, and metastasis of tumors, thus providing a theoretical basis for the precise diagnosis and treatment of tumors.

(2) In the field of regenerative medicine, noninvasive NIR-II imaging will also play an important role in exploring fundamental biological issues such as the developmental process of embryos and organs and the lineage and fate of stem cells. For instance, the complex embryonic development process in living mammals has not been fully elucidated due to the fact traditional fluorescence (400−900 nm) cannot penetrate living tissue to report embryo development *in situ*. Due to the deep tissue penetration of NIR-II imaging, the developmental dynamics of living embryos, including angiogenesis, neurogenesis, and organogenesis, may be observed by multiple spectral NIR-II imaging in combination with cell lineage tracking techniques. In addition, NIR-II imaging also has great potential for revealing the functions and fates of endogenous and exogenous stem cells. The application of multiple spectral NIR-II imaging technology may offer abundant imaging channels to simultaneously monitor the translocation, viability, paracrine, differentiation, and aging of stem cells, thus offering a comprehensive understanding of the processes and underlying mechanisms of stem cell-based regeneration.

(3) For neuroscience research, NIR-II imaging also has broad application prospects. For instance, further development of membrane potential-sensitive NIR-II probes may offer the possibility to simultaneously monitor neural activities of large numbers of nerve cell populations in deep tissues with a sub-millisecond temporal resolution and a subcellular spatial resolution. Additionally, the development of activable NIR-II probes that can specifically sense ions and neurotransmitters, such as K^+, Ca^{2+}, and dopamine, will greatly enhance research on the chemical mechanisms of neural activity. We believe these novel neural imaging techniques will not only promote the exploration of advanced neural activities (such as memory and learning), but also aid in revealing the fundamental mechanisms of neurological diseases and developing effective therapies.

(4) For clinical application, the most promising application of NIR-II imaging is image-guided tumor surgery; its superiority has just been verified by Hu and co-workers in liver-tumor surgery in human. In the future, the advanced NIR-II imaging technology may greatly improve the precision of tumor surgery and its prognosis. Moreover, NIR-II imaging-guided PDT/PTT may also be used in the clinical trials in the near further to achieve a

https://dx.doi.org/10.1021/jacs.0c07022
J. Am. Chem. Soc. 2020, 142, 14789−14804

more accurate, safe, and effective PDT/PTT for tumor treatment. In addition, with the superior performance in tissue penetration depth and spatiotemporal resolution compared to the FDA-approved ICG-based NIR-I imaging, NIR-II imaging will also have great potential in precise diagnosis and treatment of cardiovascular diseases in the clinic. Certainly, great endeavors are needed to fully promote the NIR-II imaging technology into the clinic.

AUTHOR INFORMATION

Corresponding Author

Qiangbin Wang − *CAS Key Laboratory of Nano-Bio Interface, Suzhou Key Laboratory of Functional Molecular Imaging Technology, Division of Nanobiomedicine and i-Lab, Suzhou Institute of Nano-Tech and Nano-Bionics, Chinese Academy of Sciences, Suzhou 215123, China; University of Science and Technology of China, Hefei 230036, China;* orcid.org/0000-0001-6589-6328; Email: qbwang2008@sinano.ac.cn

Authors

Chunyan Li − *CAS Key Laboratory of Nano-Bio Interface, Suzhou Key Laboratory of Functional Molecular Imaging Technology, Division of Nanobiomedicine and i-Lab, Suzhou Institute of Nano-Tech and Nano-Bionics, Chinese Academy of Sciences, Suzhou 215123, China*

Guangcun Chen − *CAS Key Laboratory of Nano-Bio Interface, Suzhou Key Laboratory of Functional Molecular Imaging Technology, Division of Nanobiomedicine and i-Lab, Suzhou Institute of Nano-Tech and Nano-Bionics, Chinese Academy of Sciences, Suzhou 215123, China;* orcid.org/0000-0002-6052-6632

Yejun Zhang − *CAS Key Laboratory of Nano-Bio Interface, Suzhou Key Laboratory of Functional Molecular Imaging Technology, Division of Nanobiomedicine and i-Lab, Suzhou Institute of Nano-Tech and Nano-Bionics, Chinese Academy of Sciences, Suzhou 215123, China*

Feng Wu − *CAS Key Laboratory of Nano-Bio Interface, Suzhou Key Laboratory of Functional Molecular Imaging Technology, Division of Nanobiomedicine and i-Lab, Suzhou Institute of Nano-Tech and Nano-Bionics, Chinese Academy of Sciences, Suzhou 215123, China*

Complete contact information is available at: https://pubs.acs.org/10.1021/jacs.0c07022

Author Contributions

‡C.L. and G.C. contributed equally.

Notes

The authors declare no competing financial interest.

ACKNOWLEDGMENTS

This work was financially supported by the National Key Research and Development Program of China (Grant Nos. 2017YFA0205503, 2016YFA0101503), the National Natural Science Foundation of China (Grant Nos. 21778070, 21703282, 21934007), the Strategic Priority Research Program of CAS (Grant No. XDB36000000), Key Research Program of Frontier Sciences, CAS (Grant No. ZDBS-LY-SLH021), and the Youth Innovation Promotion Association of CAS.

REFERENCES

(1) Weissleder, R.; Pittet, M. J. Imaging in the era of molecular oncology. *Nature* **2008**, *452* (7187), 580−589.

(2) Hong, G.; Antaris, A.; Dai, H. Near-infrared fluorophores for biomedical imaging. *Nat. Biomed. Eng.* **2017**, *1*, No. 0010.

(3) Troyan, S. L.; Kianzad, V.; Gibbs-Strauss, S. L.; Gioux, S.; Matsui, A.; Oketokoun, R.; Ngo, L.; Khamene, A.; Azar, F.; Frangioni, J. V. The FLARE intraoperative near-infrared fluorescence imaging system: a first-in-human clinical trial in breast cancer sentinel lymph node mapping. *Ann. Surg. Oncol.* **2009**, *16* (10), 2943−2952.

(4) Tummers, Q. R.; Schepers, A.; Hamming, J. F.; Kievit, J.; Frangioni, J. V.; van de Velde, C. J.; Vahrmeijer, A. L. Intraoperative guidance in parathyroid surgery using near-infrared fluorescence imaging and low-dose Methylene Blue. *Surgery* **2015**, *158* (5), 1323−1330.

(5) Welsher, K.; Liu, Z.; Sherlock, S. P.; Robinson, J. T.; Chen, Z.; Daranciang, D.; Dai, H. J. A route to brightly fluorescent carbon nanotubes for near-infrared imaging in mice. *Nat. Nanotechnol.* **2009**, *4* (11), 773−780.

(6) Smith, A. M.; Mancini, M. C.; Nie, S. Bioimaging: second window for *in vivo* imaging. *Nat. Nanotechnol.* **2009**, *4* (11), 710−711.

(7) Diao, S.; Hong, G.; Antaris, A. L.; Blackburn, J. L.; Cheng, K.; Cheng, Z.; Dai, H. Biological imaging without autofluorescence in the second near-infrared region. *Nano Res.* **2015**, *8* (9), 3027−3034.

(8) Hong, G.; Diao, S.; Chang, J.; Antaris, A. L.; Chen, C.; Zhang, B.; Zhao, S.; Atochin, D. N.; Huang, P. L.; Andreasson, K. I.; Kuo, C. J.; Dai, H. Through-skull fluorescence imaging of the brain in a new near-infrared window. *Nat. Photonics* **2014**, *8* (9), 723−730.

(9) Du, Y. P.; Xu, B.; Fu, T.; Cai, M.; Li, F.; Zhang, Y.; Wang, Q. B. Near-infrared photoluminescent Ag_2S quantum dots from a single source precursor. *J. Am. Chem. Soc.* **2010**, *132* (5), 1470−1471.

(10) Dong, B.; Li, C.; Chen, G.; Zhang, Y.; Zhang, Y.; Deng, M.; Wang, Q. Facile synthesis of highly photoluminescent Ag_2Se quantum dots as a new fluorescent probe in the second near-infrared window for *in vivo* imaging. *Chem. Mater.* **2013**, *25* (12), 2503−2509.

(11) Yang, M.; Gui, R.; Jin, H.; Wang, Z.; Zhang, F.; Xia, J.; Bi, S.; Xia, Y. Ag_2Te quantum dots with compact surface coatings of multivalent polymers: Ambient one-pot aqueous synthesis and the second near-infrared bioimaging. *Colloids Surf., B* **2015**, *126*, 115−120.

(12) Bruns, O. T.; Bischof, T. S.; Harris, D. K.; Franke, D.; Shi, Y.; Riedemann, L.; Bartelt, A.; Jaworski, F. B.; Carr, J. A.; Rowlands, C. J.; Wilson, M. W. B.; Chen, O.; Wei, H.; Hwang, G. W.; Montana, D. M.; Coropceanu, I.; Achorn, O. B.; Kloepper, J.; Heeren, J.; So, P. T. C.; Fukumura, D.; Jensen, K. F.; Jain, R. K.; Bawendi, M. G. Next-generation *in vivo* optical imaging with short-wave infrared quantum dots. *Nat. Biomed. Eng.* **2017**, *1*, No. 0056.

(13) Naczynski, D. J.; Tan, M. C.; Zevon, M.; Wall, B.; Kohl, J.; Kulesa, A.; Chen, S.; Roth, C. M.; Riman, R. E.; Moghe, P. V. Rare-earth-doped biological composites as *in vivo* shortwave infrared reporters. *Nat. Commun.* **2013**, *4*, 2199.

(14) Wang, R.; Li, X.; Zhou, L.; Zhang, F. Epitaxial seeded growth of rare-earth nanocrystals with efficient 800 nm near-infrared to 1525 nm short-wavelength infrared downconversion photoluminescence for *in vivo* bioimaging. *Angew. Chem., Int. Ed.* **2014**, *53* (45), 12086−12090.

(15) Shao, W.; Chen, G.; Kuzmin, A.; Kutscher, H. L.; Pliss, A.; Ohulchanskyy, T. Y.; Prasad, P. N. Tunable narrow band emissions from dye-sensitized core/shell/shell nanocrystals in the second near-infrared Biological Window. *J. Am. Chem. Soc.* **2016**, *138* (50), 16192−16195.

(16) Hong, G.; Zou, Y.; Antaris, A. L.; Diao, S.; Wu, D.; Cheng, K.; Zhang, X.; Chen, C.; Liu, B.; He, Y.; Wu, J. Z.; Yuan, J.; Zhang, B.; Tao, Z.; Fukunaga, C.; Dai, H. Ultrafast fluorescence imaging *in vivo* with conjugated polymer fluorophores in the second near-infrared window. *Nat. Commun.* **2014**, *5*, 4206.

(17) Shou, K.; Qu, C.; Sun, Y.; Chen, H.; Chen, S.; Zhang, L.; Xu, H.; Hong, X.; Yu, A.; Cheng, Z. Multifunctional biomedical imaging in physiological and pathological conditions using a NIR-II probe. *Adv. Funct. Mater.* **2017**, *27* (23), 1700995.

(18) Antaris, A. L.; Chen, H.; Cheng, K.; Sun, Y.; Hong, G.; Qu, C.; Diao, S.; Deng, Z.; Hu, X.; Zhang, B.; Zhang, X.; Yaghi, O. K.; Alamparambil, Z. R.; Hong, X.; Cheng, Z.; Dai, H. A small-molecule dye for NIR-II imaging. *Nat. Mater.* **2016**, *15* (2), 235−242.

(19) Li, B.; Lu, L.; Zhao, M.; Lei, Z.; Zhang, F. An efficient 1064 nm NIR-II excitation fluorescent molecular dye for deep-tissue high-resolution dynamic bioimaging. *Angew. Chem., Int. Ed.* **2018**, *57* (25), 7483−7487.
(20) Kilian, H. I.; Kang, H.; Nyayapathi, N.; Fukuda, T.; Adluru, E.; Zhang, H.; Quinn, B.; Xia, J.; Choi, H. S.; Lovell, J. F. Facile formulation of a long-wavelength cyanine for optical imaging in the second near-infrared window. *Biomater. Sci.* **2020**, *8* (15), 4199−4205.
(21) Sheng, Z.; Guo, B.; Hu, D.; Xu, S.; Wu, W.; Liew, W. H.; Yao, K.; Jiang, J.; Liu, C.; Zheng, H.; Liu, B. Bright aggregation-induced-emission dots for targeted synergetic NIR-II fluorescence and NIR-I photoacoustic imaging of orthotopic brain tumors. *Adv. Mater.* **2018**, *30*, No. e1800766.
(22) Welsher, K.; Sherlock, S. P.; Dai, H. Deep-tissue anatomical imaging of mice using carbon nanotube fluorophores in the second near-infrared window. *Proc. Natl. Acad. Sci. U. S. A.* **2011**, *108* (22), 8943−8948.
(23) Hong, G.; Lee, J. C.; Robinson, J. T.; Raaz, U.; Xie, L.; Huang, N. F.; Cooke, J. P.; Dai, H. Multifunctional *in vivo* vascular imaging using near-infrared II fluorescence. *Nat. Med.* **2012**, *18* (12), 1841−1846.
(24) Yi, H.; Ghosh, D.; Ham, M.-H.; Qi, J.; Barone, P. W.; Strano, M. S.; Belcher, A. M. M13 phage-functionalized single-walled carbon nanotubes as nanoprobes for second near-infrared window fluorescence imaging of targeted tumors. *Nano Lett.* **2012**, *12* (3), 1176−1183.
(25) Ghosh, D.; Bagley, A. F.; Na, Y. J.; Birrer, M. J.; Bhatia, S. N.; Belcher, A. M. Deep, noninvasive imaging and surgical guidance of submillimeter tumors using targeted M13-stabilized single-walled carbon nanotubes. *Proc. Natl. Acad. Sci. U. S. A.* **2014**, *111* (38), 13948−13953.
(26) Landry, M. P.; Ando, H.; Chen, A. Y.; Cao, J.; Kottadiel, V. I.; Chio, L.; Yang, D.; Dong, J.; Lu, T. K.; Strano, M. S. Single-molecule detection of protein efflux from microorganisms using fluorescent single-walled carbon nanotube sensor arrays. *Nat. Nanotechnol.* **2017**, *12*, 368−377.
(27) Bhattacharya, S.; Gong, X.; Wang, E.; Dutta, S. K.; Caplette, J. R.; Son, M.; Nguyen, F. T.; Strano, M. S.; Mukhopadhyay, D. DNA−SWCNT biosensors allow real-time monitoring of therapeutic responses in pancreatic ductal adenocarcinoma. *Cancer Res.* **2019**, *79* (17), 4515−4523.
(28) Bruchez, M., Jr.; Gin, P.; Weiss, S.; Alivisatos, A. P. Semiconductor nanocrystals as fluorescent biological labels. *Science* **1998**, *281* (5385), 2013−2016.
(29) Chan, W. C.; Nie, S. Quantum dot bioconjugates for ultrasensitive nonisotopic detection. *Science* **1998**, *281* (5385), 2016−2018.
(30) Hong, G. S.; Robinson, J. T.; Zhang, Y. J.; Diao, S.; Antaris, A. L.; Wang, Q. B.; Dai, H. J. *In vivo* fluorescence imaging with Ag_2S quantum dots in the second near-infrared region. *Angew. Chem., Int. Ed.* **2012**, *51* (39), 9818−9821.
(31) Zhang, Y.; Liu, Y.; Li, C.; Chen, X.; Wang, Q. Controlled synthesis of Ag_2S quantum dots and experimental determination of the exciton Bohr radius. *J. Phys. Chem. C* **2014**, *118*, 4918−4923.
(32) Chen, J.; Kong, Y.; Feng, S.; Chen, C.; Wo, Y.; Wang, W.; Dong, Y.; Wu, Z.; Li, Y.; Chen, S. Recycled synthesis of whey-protein-capped lead sulfide quantum dots as the second near-infrared reporter for bioimaging application. *ACS Sustainable Chem. Eng.* **2016**, *4* (6), 2932−2938.
(33) Kong, Y.; Chen, J.; Fang, H.; Heath, G.; Wo, Y.; Wang, W.; Li, Y.; Guo, Y.; Evans, S. D.; Chen, S.; Zhou, D. Highly fluorescent ribonuclease-A-encapsulated lead sulfide quantum dots for ultra-sensitive fluorescence *in vivo* imaging in the second near-infrared window. *Chem. Mater.* **2016**, *28* (9), 3041−3050.
(34) Nyk, M.; Kumar, R.; Ohulchanskyy, T. Y.; Bergey, E. J.; Prasad, P. N. High contrast *in vitro* and *in vivo* photoluminescence bioimaging using near infrared to near infrared up-conversion in Tm^{3+} and Yb^{3+} doped fluoride nanophosphors. *Nano Lett.* **2008**, *8* (11), 3834−3838.
(35) Wang, F.; Liu, X. Upconversion multicolor fine-tuning: visible to near-infrared emission from lanthanide-doped $NaYF_4$ nanoparticles. *J. Am. Chem. Soc.* **2008**, *130* (17), 5642−5643.
(36) Wang, F.; Han, Y.; Lim, C.; Lu, Y.; Wang, J.; Xu, J.; Chen, H.; Zhang, C.; Hong, M.; Liu, X. Simultaneous phase and size control of upconversion nanocrystals through lanthanide doping. *Nature* **2010**, *463*, 1061−1065.
(37) Chen, Z.; Chen, H.; Hu, H.; Yu, M.; Li, F.; Zhang, Q.; Zhou, Z.; Yi, T.; Huang, C. A versatile synthesis strategy for carboxylic acid-functionalized upconverting nanophosphors as biological labels. *J. Am. Chem. Soc.* **2008**, *130*, 3023−3029.
(38) Liu, Q.; Sun, Y.; Yang, T.; Feng, W.; Li, C.; Li, F. Sub-10 nm hexagonal lanthanide-doped $NaLuF_4$ upconversion nanocrystals for sensitive bioimaging *in vivo*. *J. Am. Chem. Soc.* **2011**, *133*, 17122−17125.
(39) Gu, Y.; Guo, Z.; Yuan, W.; Kong, M.; Liu, Y.; Liu, Y.; Gao, Y.; Feng, W.; Wang, F.; Zhou, J.; Jin, D.; Li, F. High-sensitivity imaging of time-domain near-infrared light transducer. *Nat. Photonics* **2019**, *13*, 525−531.
(40) Zhang, F.; Shi, Q.; Zhang, Y.; Shi, Y.; Ding, K.; Zhao, D.; Stucky, G. D. Fluorescence upconversion microbarcodes for multiplexed biological detection: nucleic acid encoding. *Adv. Mater.* **2011**, *23* (33), 3775−3779.
(41) Zhang, F.; Braun, G.; Pallaoro, A.; Zhang, Y.; Shi, Y.; Cui, D.; Moskovits, M.; Zhao, D.; Stucky, G. Mesoporous multifunctional upconversion luminescent and magnetic "nanorattle" materials for targeted chemotherapy. *Nano Lett.* **2012**, *12*, 61−67.
(42) Carr, J. A.; Franke, D.; Caram, J. R.; Perkinson, C. F.; Saif, M.; Askoxylakis, V.; Datta, M.; Fukumura, D.; Jain, R. K.; Bawendi, M. G.; Bruns, O. T. Shortwave infrared fluorescence imaging with the clinically approved near-infrared dye indocyanine green. *Proc. Natl. Acad. Sci. U. S. A.* **2018**, *115* (17), 4465−4470.
(43) Sun, C.; Li, B.; Zhao, M.; Wang, S.; Lei, Z.; Lu, L.; Zhang, H.; Feng, L.; Dou, C.; Yin, D.; Xu, H.; Cheng, Y.; Zhang, F. J-aggregates of cyanine dye for NIR-II *in vivo* dynamic vascular imaging beyond 1500 nm. *J. Am. Chem. Soc.* **2019**, *141* (49), 19221−19225.
(44) Antaris, A. L.; Chen, H.; Diao, S.; Ma, Z.; Zhang, Z.; Zhu, S.; Wang, J.; Lozano, A. X.; Fan, Q.; Chew, L.; Zhu, M.; Cheng, K.; Hong, X.; Dai, H.; Cheng, Z. A high quantum yield molecule-protein complex fluorophore for near-infrared II imaging. *Nat. Commun.* **2017**, *8*, 15269.
(45) Sun, Y.; Qu, C.; Chen, H.; He, M.; Tang, C.; Shou, K.; Hong, S.; Yang, M.; Jiang, Y.; Ding, B.; Xiao, Y.; Xing, L.; Hong, X.; Cheng, Z. Novel benzo-bis(1,2,5-thiadiazole) fluorophores for *in vivo* NIR-II imaging of cancer. *Chem. Sci.* **2016**, *7* (9), 6203−6207.
(46) Sun, Y.; Zeng, X.; Xiao, Y.; Liu, C.; Zhu, H.; Zhou, H.; Chen, Z.; Xu, F.; Wang, J.; Zhu, M.; Wu, J.; Tian, M.; Zhang, H.; Deng, Z.; Cheng, Z.; Hong, X. Novel dual-function near-infrared II fluorescence and PET probe for tumor delineation and image-guided surgery. *Chem. Sci.* **2018**, *9* (8), 2092−2097.
(47) Zhang, X. D.; Wang, H.; Antaris, A. L.; Li, L.; Diao, S.; Ma, R.; Nguyen, A.; Hong, G.; Ma, Z.; Wang, J.; Zhu, S.; Castellano, J. M.; Wyss-Coray, T.; Liang, Y.; Luo, J.; Dai, H. Traumatic brain injury imaging in the second near-infrared window with a molecular fluorophore. *Adv. Mater.* **2016**, *28* (32), 6872−6879.
(48) Miao, Q.; Pu, K. Organic semiconducting agents for deep-tissue molecular imaging: second near-infrared gluorescence, self-luminescence, and photoacoustics. *Adv. Mater.* **2018**, *30* (49), 1801778.
(49) Jiang, Y.; Upputuri, P. K.; Xie, C.; Lyu, Y.; Zhang, L.; Xiong, Q.; Pramanik, M.; Pu, K. Broadband absorbing semiconducting polymer nanoparticles for photoacoustic imaging in second near-infrared window. *Nano Lett.* **2017**, *17* (8), 4964−4969.
(50) Huang, J.; Xie, C.; Zhang, X.; Jiang, Y.; Li, J.; Fan, Q.; Pu, K. Renal-clearable molecular semiconductor for second near-infrared fluorescence imaging of kidney dysfunction. *Angew. Chem., Int. Ed.* **2019**, *58* (42), 15120−15127.
(51) He, S.; Jiang, Y.; Li, J.; Pu, K. Semiconducting polycomplex nanoparticles for photothermal ferrotherapy of cancer. *Angew. Chem., Int. Ed.* **2020**, *59* (26), 10633−10638.
(52) Luo, J. D.; Xie, Z. L.; Lam, J. W. Y.; Cheng, L.; Chen, H. Y.; Qiu, C. F.; Kwok, H. S.; Zhan, X. W.; Liu, Y. Q.; Zhu, D. B.; Tang, B. Z. Aggregation-induced emission of 1-methyl-1,2,3,4,5-pentaphenylsilole. *Chem. Commun.* **2001**, No. 18, 1740−1741.

https://dx.doi.org/10.1021/jacs.0c07022
J. Am. Chem. Soc. 2020, 142, 14789−14804

(53) Li, Y.; Cai, Z.; Liu, S.; Zhang, H.; Wong, S.; Lam, J.; Kwok, R.; Qian, J.; Tang, B. Design of AIEgens for near-infrared IIb imaging through structural modulation at molecular and morphological levels. *Nat. Commun.* **2020**, *11*, 1255.
(54) Liu, S.; Li, Y.; Kwok, R. T. K.; Lam, J. W. Y.; Tang, B. Z. Structural and process controls of AIEgens for NIR-II theranostics. *Chem. Sci.* **2020**, DOI: 10.1039/D0SC02911D.
(55) Lu, H.; Carroll, G. M.; Neale, N. R.; Beard, M. C. Infrared quantum dots: progress, challenges and opportunities. *ACS Nano* **2019**, *13* (2), 939−953.
(56) Zhang, Y.; Zhang, Y.; Hong, G.; He, W.; Zhou, K.; Yang, K.; Li, F.; Chen, G.; Liu, Z.; Dai, H.; Wang, Q. Biodistribution, pharmacokinetics and toxicology of Ag_2S near-infrared quantum dots in mice. *Biomaterials* **2013**, *34* (14), 3639−3646.
(57) Huang, D.; Lin, S.; Wang, Q.; Zhang, Y.; Li, C.; Ji, R.; Wang, M.; Chen, G.; Wang, Q. An NIR-II fluorescence/dual bioluminescence multiplexed imaging for *in vivo* visualizing the location, survival, and differentiation of transplanted stem cells. *Adv. Funct. Mater.* **2019**, *29* (2), 1806546.
(58) Fan, Y.; Wang, P.; Lu, Y.; Wang, R.; Zhou, L.; Zheng, X.; Li, X.; Piper, J. A.; Zhang, F. Lifetime-engineered NIR-II nanoparticles unlock multiplexed *in vivo* imaging. *Nat. Nanotechnol.* **2018**, *13* (10), 941−946.
(59) Hu, Z.; Fang, C.; Li, B.; Zhang, Z.; Cao, C.; Cai, M.; Su, S.; Sun, X.; Shi, X.; Li, C.; Zhou, T.; Zhang, Y.; Chi, C.; He, P.; Xia, X.; Chen, Y.; Gambhir, S. S.; Cheng, Z.; Tian, J. First-in-human liver-tumour surgery guided by multispectral fluorescence imaging in the visible and near-infrared-I/II windows. *Nat. Biomed. Eng.* **2020**, *4* (3), 259−271.
(60) Del Bonis-O'Donnell, J.; Page, R.; Beyene, A.; Tindall, E.; McFarlane, I.; Landry, M. Dual near-infrared two-photon microscopy for deep-tissue dopamine nanosensor imaging. *Adv. Funct. Mater.* **2017**, *27* (39), 1702112.
(61) Zhu, S.; Herraiz, S.; Yue, J.; Zhang, M.; Wan, H.; Yang, Q.; Ma, Z.; Wang, Y.; He, J.; Antaris, A. L.; Zhong, Y.; Diao, S.; Feng, Y.; Zhou, Y.; Yu, K.; Hong, G.; Liang, Y.; Hsueh, A. J.; Dai, H. 3D NIR-II molecular imaging distinguishes targeted organs with high-performance NIR-II bioconjugates. *Adv. Mater.* **2018**, *30* (13), No. e1705799.
(62) Wang, F.; Wan, H.; Ma, Z.; Zhong, Y.; Sun, Q.; Tian, Y.; Qu, L.; Du, H.; Zhang, M.; Li, L.; Ma, H.; Luo, J.; Liang, Y.; Li, W. J.; Hong, G.; Liu, L.; Dai, H. Light-sheet microscopy in the near-infrared II window. *Nat. Methods* **2019**, *16* (6), 545−552.
(63) Chen, G.; Lin, S.; Huang, D.; Zhang, Y.; Li, C.; Wang, M.; Wang, Q. Revealing the fate of transplanted stem cells *in vivo* with a novel optical imaging strategy. *Small* **2018**, *14* (3), 1702679.
(64) Hao, X.; Li, C.; Zhang, Y.; Wang, H.; Chen, G.; Wang, M.; Wang, Q. Programmable Chemotherapy and Immunotherapy against Breast Cancer Guided by Multiplexed Fluorescence Imaging in the Second Near-Infrared Window. *Adv. Mater.* **2018**, *30* (51), No. e1804437.
(65) Li, C.; Zhang, Y.; Wang, M.; Zhang, Y.; Chen, G.; Li, L.; Wu, D.; Wang, Q. *In vivo* real-time visualization of tissue blood flow and angiogenesis using Ag_2S quantum dots in the NIR-II window. *Biomaterials* **2014**, *35* (1), 393−400.
(66) Guo, B.; Feng, Z.; Hu, D.; Xu, S.; Middha, E.; Pan, Y.; Liu, C.; Zheng, H.; Qian, J.; Sheng, Z.; Liu, B. Precise deciphering of brain vasculatures and microscopic tumors with dual NIR-II fluorescence and photoacoustic imaging. *Adv. Mater.* **2019**, *31* (30), No. e1902504.
(67) Zhang, Z.; Fang, X.; Liu, Z.; Liu, H.; Chen, D.; He, S.; Zheng, J.; Yang, B.; Qin, W.; Zhang, X.; Wu, C. Semiconducting polymer dots with dual-enhanced NIR-IIa fluorescence for through-skull mouse-brain imaging. *Angew. Chem., Int. Ed.* **2020**, *59* (9), 3691−3698.
(68) Cai, Z. C.; Zhu, L.; Wang, M. Q.; Roe, A. W.; Xi, W.; Qian, J. NIR-II fluorescence microscopic imaging of cortical vasculature in non-human primates. *Theranostics* **2020**, *10* (9), 4265−4276.
(69) Tanaka, E.; Chen, F. Y.; Flaumenhaft, R.; Graham, G. J.; Laurence, R. G.; Frangioni, J. V. Real-time assessment of cardiac perfusion, coronary angiography, and acute intravascular thrombi using dual-channel near-infrared fluorescence imaging. *J. Thorac. Cardiovasc. Surg.* **2009**, *138* (1), 133−140.
(70) Li, C.; Cao, L.; Zhang, Y.; Yi, P.; Wang, M.; Tan, B.; Deng, Z.; Wu, D.; Wang, Q. Preoperative detection and intraoperative visualization of brain tumors for more precise surgery: a new dual-modality MRI and NIR nanoprobe. *Small* **2015**, *11* (35), 4517−4525.
(71) Liu, S. J.; Chen, C.; Li, Y. Y.; Zhang, H. K.; Liu, J. K.; Wang, R.; Wong, S. T. H.; Lam, J. W. Y.; Ding, D.; Tang, B. Constitutional isomerization enables bright NIR-II AIEgen for brain-inflammation imaging. *Adv. Funct. Mater.* **2020**, *30* (7), 1908125.
(72) Wan, H.; Yue, J.; Zhu, S.; Uno, T.; Zhang, X.; Yang, Q.; Yu, K.; Hong, G.; Wang, J.; Li, L.; Ma, Z.; Gao, H.; Zhong, Y.; Su, J.; Antaris, A. L.; Xia, Y.; Luo, J.; Liang, Y.; Dai, H. A bright organic NIR-II nanofluorophore for three-dimensional imaging into biological tissues. *Nat. Commun.* **2018**, *9* (1), 1171.
(73) Mieog, J. S.; Troyan, S. L.; Hutteman, M.; Donohoe, K. J.; van der Vorst, J. R.; Stockdale, A.; Liefers, G. J.; Choi, H. S.; Gibbs-Strauss, S. L.; Putter, H.; Gioux, S.; Kuppen, P. J.; Ashitate, Y.; Lowik, C. W.; Smit, V. T.; Oketokoun, R.; Ngo, L. H.; van de Velde, C. J.; Frangioni, J. V.; Vahrmeijer, A. L. Toward optimization of imaging system and lymphatic tracer for near-infrared fluorescent sentinel lymph node mapping in breast cancer. *Ann. Surg. Oncol.* **2011**, *18* (9), 2483−2491.
(74) Li, C.; Wang, Q. Advanced NIR-II fluorescence imaging technology for *in vivo* precision tumor theranostics. *Adv. Therap.* **2019**, *2* (9), 1900053.
(75) Li, Y. B.; Zeng, S. J.; Hao, J. H. Non-invasive optical guided tumor metastasis/vessel imaging by using lanthanide nanoprobe with enhanced down-shifting emission beyond 1500 nm. *ACS Nano* **2019**, *13* (1), 248−259.
(76) Zhang, Z.; Chen, D.; Liu, Z.; Wang, D.; Guo, J.; Zheng, J.; Qin, W.; Wu, C. Near-infrared polymer dots with aggregation-induced emission for tumor imaging. *ACS Appl. Polym. Mater.* **2020**, *2* (1), 74−79.
(77) Chen, G.; Cao, Y.; Tang, Y.; Yang, X.; Liu, Y.; Huang, D.; Zhang, Y.; Li, C.; Wang, Q. Advanced near-infrared light for monitoring and modulating the spatiotemporal dynamics of cell functions in living systems. *Adv. Sci.* **2020**, *7* (8), 1903783.
(78) Hong, G.; Lee, J. C.; Jha, A.; Diao, S.; Nakayama, K. H.; Hou, L.; Doyle, T. C.; Robinson, J. T.; Antaris, A. L.; Dai, H.; Cooke, J. P.; Huang, N. F. Near-infrared II fluorescence for imaging hindlimb vessel regeneration with dynamic tissue perfusion measurement. *Circ. Cardiovasc. Imaging* **2014**, *7* (3), 517−525.
(79) Wan, H.; Du, H.; Wang, F.; Dai, H. Molecular imaging in the second near-infrared window. *Adv. Funct. Mater.* **2019**, *29* (25), 1900566.
(80) Huang, J.; Pu, K. Activatable molecular probes for second near-infrared fluorescence, chemiluminescence, and photoacoustic imaging. *Angew. Chem., Int. Ed.* **2020**, *59* (29), 11717−11731.
(81) Tang, Y. F.; Pei, F.; Lu, X. M.; Fan, Q. L.; Huang, W. Recent advances on activatable NIR-II fluorescence probes for biomedical imaging. *Adv. Opt. Mater.* **2019**, *7* (21), e1900917.
(82) Lou, Z. R.; Li, P.; Han, K. L. Redox-responsive fluorescent probes with different design strategies. *Acc. Chem. Res.* **2015**, *48* (5), 1358−1368.
(83) Tang, Y. F.; Li, Y. Y.; Wang, Z.; Pei, F.; Hu, X. M.; Ji, Y.; Li, X.; Zhao, H.; Hu, W. B.; Lu, X. M.; Fan, Q. L.; Huang, W. Organic semiconducting nanoprobe with redox-activatable NIR-II fluorescence for *in vivo* real-time monitoring of drug toxicity. *Chem. Commun.* **2019**, *55* (1), 27−30.
(84) Lei, X.; Li, R.; Tu, D.; Shang, X.; Liu, Y.; You, W.; Sun, C.; Zhang, F.; Chen, X. Intense near-infrared-II luminescence from $NaCeF_4$:Er/Yb nanoprobes for *in vitro* bioassay and *in vivo* bioimaging. *Chem. Sci.* **2018**, *9* (20), 4682−4688.
(85) Tang, Y. F.; Li, Y. Y.; Lu, X. M.; Hu, X. M.; Zhao, H.; Hu, W. B.; Lu, F.; Fan, Q. L.; Huang, W. Bio-erasable intermolecular donor-acceptor interaction of organic semiconducting nanoprobes for activatable NIR-II fluorescence imaging. *Adv. Funct. Mater.* **2019**, *29* (10), 1807376.
(86) Li, D.; Wang, S.; Lei, Z.; Sun, C.; El-Toni, A. M.; Alhoshan, M. S.; Fan, Y.; Zhang, F. Peroxynitrite activatable NIR-II fluorescent molecular probe for drug-induced hepatotoxicity monitoring. *Anal. Chem.* **2019**, *91* (7), 4771−4779.

(87) Lei, Z.; Sun, C.; Pei, P.; Wang, S.; Li, D.; Zhang, X.; Zhang, F. Stable, wavelength-tunable fluorescent dyes in the NIR-II region for *in vivo* high-contrast bioimaging and multiplexed biosensing. *Angew. Chem., Int. Ed.* **2019**, *58* (24), 8166−8171.
(88) Li, C.; Li, W.; Liu, H.; Zhang, Y.; Chen, G.; Li, Z.; Wang, Q. An activatable NIR-II nanoprobe for *in vivo* early real-time diagnosis of traumatic brain injury. *Angew. Chem., Int. Ed.* **2020**, *59* (1), 247−252.
(89) Tang, Y.; Li, Y.; Hu, X.; Zhao, H.; Ji, Y.; Chen, L.; Hu, W.; Zhang, W.; Li, X.; Lu, X.; Huang, W.; Fan, Q. "Dual Lock-and-Key"-controlled nanoprobes for ultrahigh specific fluorescence imaging in the second near-Infrared window. *Adv. Mater.* **2018**, *30* (31), No. e1801140.
(90) Benayas, A.; Ren, F. Q.; Carrasco, E.; Marzal, V.; del Rosal, B.; Gonfa, B. A.; Juarranz, A.; Sanz-Rodriguez, F.; Jaque, D.; Garcia-Sole, J.; Ma, D. L.; Vetrone, F. PbS/CdS/ZnS quantum dots: a multifunctional platform for *in vivo* near-infrared low-dose fluorescence imaging. *Adv. Funct. Mater.* **2015**, *25* (42), 6650−6659.
(91) Xu, G.; Yan, Q.; Lv, X.; Zhu, Y.; Xin, K.; Shi, B.; Wang, R.; Chen, J.; Gao, W.; Shi, P.; Fan, C.; Zhao, C.; Tian, H. Imaging of colorectal cancers using activatable nanoprobes with second near-infrared window emission. *Angew. Chem., Int. Ed.* **2018**, *57* (14), 3626−3630.
(92) Iverson, N. M.; Barone, P. W.; Shandell, M.; Trudel, L. J.; Sen, S.; Sen, F.; Ivanov, V.; Atolia, E.; Farias, E.; McNicholas, T. P.; Reuel, N.; Parry, N. M. A.; Wogan, G. N.; Strano, M. S. *In vivo* biosensing via tissue-localizable near-infrared-fluorescent single-walled carbon nanotubes. *Nat. Nanotechnol.* **2013**, *8* (11), 873−880.
(93) Wang, S.; Fan, Y.; Li, D.; Sun, C.; Lei, Z.; Lu, L.; Wang, T.; Zhang, F. Anti-quenching NIR-II molecular fluorophores for in vivo high-contrast imaging and pH sensing. *Nat. Commun.* **2019**, *10* (1), 1058.
(94) Jeong, S.; Song, I.; Lee, W.; Ryu, Y. M.; Jung, Y.; Kim, S. Y.; Kim, K.; Hong, S. C.; Myung, S. J.; Kim, S. Cancer-microenvironment-sensitive activatable quantum dot probe in the second near-infrared window. *Nano Lett.* **2017**, *17* (3), 1378−1386.
(95) Yan, R.; Hu, Y.; Liu, F.; Wei, S.; Fang, D.; Shuhendler, A. J.; Liu, H.; Chen, H. Y.; Ye, D. Activatable NIR fluorescence/MRI bimodal probes for *in vivo* imaging by enzyme-mediated fluorogenic reaction and self-assembly. *J. Am. Chem. Soc.* **2019**, *141* (26), 10331−10341.
(96) Meng, X. Q.; Zhang, J. L.; Sun, Z. H.; Zhou, L. H.; Deng, G. J.; Li, S. P.; Li, W. J.; Gong, P.; Cai, L. T. Hypoxia-triggered single molecule probe for high-contrast NIR II/PA tumor imaging and robust photothermal therapy. *Theranostics* **2018**, *8* (21), 6025−6034.
(97) Chen, G.; Zhang, Y.; Li, C.; Huang, D.; Wang, Q.; Wang, Q. Recent advances in tracking the transplanted stem cells using near-infrared fluorescent nanoprobes: turning from the first to the second near-infrared window. *Adv. Healthcare Mater.* **2018**, *7* (20), No. e1800497.
(98) Zhu, S.; Tian, R.; Antaris, A. L.; Chen, X.; Dai, H. Near-Infrared-II molecular dyes for cancer imaging and surgery. *Adv. Mater.* **2019**, *31* (24), No. e1900321.
(99) Chen, G.; Tian, F.; Zhang, Y.; Zhang, Y.; Li, C.; Wang, Q. Tracking of transplanted human mesenchymal stem cells in living mice using near-infrared Ag_2S quantum dots. *Adv. Funct. Mater.* **2014**, *24* (17), 2481−2488.
(100) Chen, G.; Tian, F.; Li, C.; Zhang, Y.; Weng, Z.; Zhang, Y.; Peng, R.; Wang, Q. *In vivo* real-time visualization of mesenchymal stem cells tropism for cutaneous regeneration using NIR-II fluorescence imaging. *Biomaterials* **2015**, *53*, 265−273.
(101) Yang, Y. M.; Chen, J.; Shang, X. L.; Feng, Z. J.; Chen, C.; Lu, J. Y.; Cai, J. Y.; Chen, Y. Z.; Zhang, J.; Hao, Y. F.; Yang, X.; Li, Y. X.; Chen, S. Y. Visualizing the fate of intra-articular injected mesenchymal stem cells *in vivo* in the second near-infrared window for the effective treatment of supraspinatus tendon tears. *Adv. Sci.* **2019**, *6* (19), No. e1901018.
(102) Hu, F.; Li, C.; Zhang, Y.; Wang, M.; Wu, D.; Wang, Q. Real-time *in vivo* visualization of tumor therapy by a near-infrared-II Ag_2S quantum dot-based theranostic nanoplatform. *Nano Res.* **2015**, *8* (5), 1637−1647.
(103) Li, C.; Li, F.; Zhang, Y.; Zhang, W.; Zhang, X. E.; Wang, Q. Real-time monitoring surface chemistry-dependent *in vivo* behaviors of protein nanocages via encapsulating an NIR-II Ag_2S quantum dot. *ACS Nano* **2015**, *9* (12), 12255−12263.
(104) Song, C.; Zhang, Y.; Li, C.; Chen, G.; Kang, X.; Wang, Q. Enhanced nanodrug delivery to solid tumors based on a tumor vasculature-targeted strategy. *Adv. Funct. Mater.* **2016**, *26* (23), 4192−4200.
(105) Li, C.; Zhang, Y.; Chen, G.; Hu, F.; Zhao, K.; Wang, Q. Engineered multifunctional nanomedicine for simultaneous stereotactic chemotherapy and inhibited osteolysis in an orthotopic model of bone metastasis. *Adv. Mater.* **2017**, *29* (13), 1605754.
(106) Ling, S.; Yang, X.; Li, C.; Zhang, Y.; Yang, H.; Chen, G.; Wang, Q. Tumor microenvironment-activated NIR-II nanotheranostic system for precise diagnosis and treatment of peritoneal metastasis. *Angew. Chem., Int. Ed.* **2020**, *59* (18), 7219−7223.
(107) Zeng, X.; Xie, L.; Chen, D.; Li, S.; Nong, J.; Wang, B.; Tang, L.; Li, Q.; Li, Y.; Deng, Z.; Hong, X.; Wu, M.; Xiao, Y. A bright NIR-II fluorescent probe for breast carcinoma imaging and image-guided surgery. *Chem. Commun.* **2019**, *55* (95), 14287−14290.
(108) Zhang, X.; Ding, B.; Qu, C.; Li, H.; Sun, Y.; Gai, Y.; Chen, H.; Fang, H.; Qian, K.; Zhang, Y.; Cheng, Z.; Lan, X. A thiopyrylium salt for PET/NIR-II tumor imaging and image-guided surgery. *Mol. Oncol.* **2020**, *14* (5), 1089−1100.
(109) Zhang, X.; He, S.; Ding, B.; Qu, C.; Zhang, Q.; Chen, H.; Sun, Y.; Fang, H.; Long, Y.; Zhang, R.; Lan, X.; Cheng, Z. Cancer cell membrane-coated rare earth doped nanoparticles for tumor surgery navigation in NIR-II imaging window. *Chem. Eng. J.* **2020**, *385*, 123959.
(110) Wen, Q.; Zhang, Y.; Li, C.; Ling, S.; Yang, X.; Chen, G.; Yang, Y.; Wang, Q. NIR-II fluorescent self-assembled peptide nanochain for ultrasensitive detection of peritoneal metastasis. *Angew. Chem., Int. Ed.* **2019**, *58* (32), 11001−11006.
(111) Liang, C.; Diao, S.; Wang, C.; Gong, H.; Liu, T.; Hong, G.; Shi, X.; Dai, H.; Liu, Z. Tumor metastasis inhibition by imaging-guided photothermal therapy with single-walled carbon nanotubes. *Adv. Mater.* **2014**, *26* (32), 5646−5652.
(112) Jiang, Y.; Li, J.; Zhen, X.; Xie, C.; Pu, K. Dual-peak absorbing semiconducting copolymer nanoparticles for first and second near-infrared window photothermal therapy: a comparative study. *Adv. Mater.* **2018**, *30* (14), No. e1705980.
(113) Liu, Y. J.; Bhattarai, P.; Dai, Z. F.; Chen, X. Y. Photothermal therapy and photoacoustic imaging via nanotheranostics in fighting cancer. *Chem. Soc. Rev.* **2019**, *48* (7), 2053−2108.
(114) Li, T.; Li, C.; Ruan, Z.; Xu, P.; Yang, X.; Yuan, P.; Wang, Q.; Yan, L. Polypeptide-conjugated second near-infrared organic fluorophore for image-guided photothermal therapy. *ACS Nano* **2019**, *13* (3), 3691−3702.
(115) Gao, S.; Wei, G. G.; Zhang, S. H.; Zheng, B. B.; Xu, J. J.; Chen, G. X.; Li, M. W.; Song, S. L.; Fu, W.; Xiao, Z. Y.; Lu, W. Albumin tailoring fluorescence and photothermal conversion effect of near-infrared-II fluorophore with aggregation-induced emission characteristics. *Nat. Commun.* **2019**, *10* (1), 2206.
(116) Shi, B.; Yan, Q.; Tang, J.; Xin, K.; Zhang, J.; Zhu, Y.; Xu, G.; Wang, R.; Chen, J.; Gao, W.; Zhu, T.; Shi, J.; Fan, C.; Zhao, C.; Tian, H. Hydrogen sulfide-activatable second near-infrared fluorescent nanoassemblies for targeted photothermal cancer therapy. *Nano Lett.* **2018**, *18* (10), 6411−6416.
(117) Wang, P.; Wang, X.; Luo, Q.; Li, Y.; Lin, X.; Fan, L.; Zhang, Y.; Liu, J.; Liu, X. Fabrication of red blood cell-based multimodal theranostic probes for second near-infrared window fluorescence imaging-guided tumor surgery and photodynamic therapy. *Theranostics* **2019**, *9* (2), 369−380.
(118) Suo, Y.; Wu, F.; Xu, P.; Shi, H.; Wang, T.; Liu, H.; Cheng, Z. NIR-II fluorescence endoscopy for targeted imaging of colorectal cancer. *Adv. Healthcare Mater.* **2019**, *8* (23), No. e1900974.

https://dx.doi.org/10.1021/jacs.0c07022
J. Am. Chem. Soc. 2020, 142, 14789−14804